Journal of Geodesy (2021) 95:91
https://doi.org/10.1007/s00190-021-01546-0

ORIGINAL ARTICLE

Integer-estimable FDMA model as an enabler of GLONASS PPP-RTK

Baocheng Zhang[1] · **Pengyu Hou**[1,2] · **Jiuping Zha**[1,2] · **Teng Liu**[1]

Received: 8 January 2021 / Accepted: 14 July 2021 / Published online: 26 July 2021

Abstract
PPP-RTK extends the precise point positioning (PPP) concept by incorporating the idea of integer ambiguity resolution underlying the real-time kinematic (RTK) technique, making rapid initialization and high accuracy attainable with a standalone receiver. While PPP-RTK has been well achieved by using global navigation satellite system code division multiple access observables, GLONASS PPP-RTK is nonetheless challenging due to the nature of frequency division multiple access (FDMA) observables. In this work, we present a GLONASS PPP-RTK concept that takes advantage of the integer-estimable FDMA (IE-FDMA) model recently proposed in Teunissen (in GPS Solut 23(4):1–19, 2019. https://doi.org/10.1007/s10291-019-0889-0) to guarantee rigorous integer ambiguity resolution and simultaneously takes care of the presence of the inter-frequency biases (IFBs) in homogeneous and heterogeneous network configurations. When conducting GLONASS PPP-RTK based on a network of homogeneous receivers, code and phase observation equations are used to construct the IE-FDMA model, in which the IFBs are implicitly eliminated through reparameterization. For a network consisting of heterogeneous receivers, we exclude the code observables and develop a phase-only IE-FDMA model instead, thereby circumventing the adverse effects of IFBs. For verification purposes, we collect a set of five-day global positioning system (GPS) and GLONASS data from two regional networks: one equipped with homogeneous receivers and another with heterogeneous receivers. The results show that the GLONASS-specific network corrections, including satellite clocks, satellite phase biases, and ionospheric delays estimated by the two networks, are as precise as those of their GPS-specific counterparts. Via satellite clock and phase bias corrections, we succeed in fixing both GPS and GLONASS ambiguities, shortening the convergence time to 5 (12) min, compared to 11 (18) min of ambiguity-float positioning in the case of a homogeneous (heterogeneous) network with a data sampling rate of 30 s. For ambiguity-fixed positioning, the convergence time defined in this work also indicates the time to first fix since the positioning error converges to the centimeter level once successful integer ambiguity resolution is achieved. Adding ionospheric corrections further speeds up the initialization in the two networks, with the convergence time being reduced to 0.5 (3) min. Compared with GPS-only positioning, the integration of GPS and GLONASS yields an improvement of 8–34% in accuracy and leads to a reduction of 25–50% in convergence.

Keywords GLONASS · PPP-RTK · Integer-estimability · Frequency division multiple access (FDMA) · Inter-frequency bias (IFB) · Integer ambiguity resolution (IAR)

1 Introduction

PPP-RTK inherits the service mode of the precise point positioning (PPP) concept and simultaneously incorporates the idea of integer ambiguity resolution underlying the real-time kinematic (RTK) technique, enabling single-receiver users to rapidly achieve high-accuracy positioning (Wübbena et al. 2005). Pioneering studies revealed the principles of PPP-RTK and demonstrated it by using global positioning system (GPS) observables (Collins et al. 2010; Ge et al. 2008; Laurichesse et al. 2009; Teunissen et al. 2010; Zhang et al. 2011). The advent of other global navigation satellite

✉ Baocheng Zhang
b.zhang@whigg.ac.cn

[1] State Key Laboratory of Geodesy and Earth's Dynamics, Innovation Academy for Precision Measurement Science and Technology, Chinese Academy of Sciences, Wuhan, China

[2] College of Earth and Planetary Sciences, University of Chinese Academy of Sciences, Beijing, China

systems (GNSSs), such as the Chinese BeiDou and the European Galileo, has led to the prevalence of multi-GNSS PPP-RTK (Hu et al. 2020; Khodabandeh and Teunissen 2016; Li et al. 2018). The integration of multi-GNSS enhances the receiver-to-satellite geometry and increases the redundancy, thus shortening the convergence time and improving the positioning accuracy (Leick et al. 2015; Teunissen and Montenbruck 2017). However, taking into consideration the observables of GLONASS is particularly challenging since it is the only system that adopts frequency division multiple access (FDMA) modulation.

The FDMA technique defines 14 different frequencies to identify GLONASS satellites, resulting in the presence of inter-frequency biases (IFBs) in both the phase and code observables. Generally, the phase IFBs are stable and bear a linear relation with the channel number and thus can either be calibrated a priori or well modeled (Reussner and Wanninger 2011; Tian et al. 2015; Wanninger 2012). More typically, studies demonstrate that the between-receiver differential phase IFBs are small enough to be neglected in most practical cases (Sleewagen 2012; Teunissen 2019). However, the code IFBs can reach several meters and differ in not only receiver type but also antennas and firmware (Al-Shaery et al. 2013; Yamada et al. 2010). As a result, the ignorance of differential code IFBs works only between homogeneous receivers of which the connected antenna and firmware are also of the same type (Kozlov et al. 2000; Reussner and Wanninger 2011). However, in the case of heterogeneous receivers, a very large table of code IFBs consisting of all combinations of receivers, antennas, and firmware is needed for calibration. Note that, for brevity, homogeneous receivers in the following refer to a configuration involving receivers, antennas, and firmware of the same type.

To prevent IFBs from undermining the integer property of ambiguities, the existing GLONASS PPP-RTK methods adopt different strategies. Here and in the following, we divide, according to whether a priori calibration of IFBs is required, the GLONASS PPP-RTK methods into two categories: IFB-calibrated and IFB-free methods. In a network equipped with homogeneous receivers, the GLONASS PPP-RTK should be conducted by employing the IFB-free methods, in which the IFBs are implicitly eliminated through reparameterization, thus avoiding external calibration (Liu et al. 2017). When considering the case generally encountered in practice, where the receivers equipped in a network are heterogeneous, one can turn to the IFB-calibrated methods, provided that an all-inclusive IFB look-up table is accessible (Reussner and Wanninger 2011). To relieve this restriction, an alternative method imposes external ionospheric constraints to prevent the IFBs from propagating into ambiguities, in an attempt to achieve an IFB-free method (Geng and Bock 2016). The other IFB-free method (Banville et al. 2013a, b), independent of any external information, estimates the linear IFBs on the fly, although studies have indicated that the code IFBs could have a nonlinear response to the channel number (Reussner and Wanninger 2011).

Another difficulty underlying GLONASS PPP-RTK is the formulation of estimable integer ambiguities. As clarified in Teunissen and Khodabandeh (2015), code division multiple access (CDMA) PPP-RTK fixes, no matter what methods are adopted, double-differenced ambiguities but neither undifferenced nor single-differenced ones. The formation of double-differenced ambiguities is straightforward for CDMA systems, whereas the different wavelengths of GLONASS satellites in common view hinder this process, resulting in a rank-deficient system. The existing GLONASS PPP-RTK methods, including both IFB-calibrated and IFB-free categories, succeed in constructing estimable ambiguities in integer form. For instance, Banville et al. (2013a) formed GLONASS estimable ambiguities by selecting two reference satellites with adjacent channel numbers. However, a new integer-estimable FDMA (IE-FDMA) model, proposed recently in Teunissen (2019), indicates that the condition of integerness of estimable ambiguities is not sufficient to achieve ambiguity resolution. A rigorous model should also ensure, as the IE-FDMA model does, the integerness of the original undifferenced ambiguities such that the model is constrained to physical consistency. Preliminary studies of the IE-FDMA model achieved fast ambiguity resolution in RTK positioning and demonstrated that the model is generally applicable (Brack et al. 2020; Hou et al. 2020; Teunissen and Khodabandeh 2019). Of great interest is how the IE-FDMA model can be applied to GLONASS PPP-RTK, which is investigated in this work.

To develop the IE-FDMA PPP-RTK model, we prefer to use as our foundation the undifferenced and uncombined method due to its several benefits (Odijk et al. 2012; Teunissen et al. 2010; Zhang et al. 2011). For instance, it enables joint processing of data from an arbitrary number of frequencies and systems (Odijk et al. 2016; Schönemann et al. 2011), which is promising for multi-frequency and multi-GNSS data processing and thus beneficial for integrating GLONASS with other systems. Taking the effects of IFBs into account, we propose an IFB-free solution. More specifically, when conducting GLONASS PPP-RTK based on a network of homogeneous receivers, we provide insights into how the code and phase IFBs are implicitly eliminated in the context of undifferenced and uncombined data processing. For a network consisting of heterogeneous receivers, we exclude the code observables and derive a phase-only IE-FDMA model, which circumvents the inverse effects of IFBs.

The remainder of this paper proceeds as follows. Section 2 revisits the code-plus-phase CDMA PPP-RTK model and extends it to FDMA observables, making it applicable for homogeneous network configurations. For a network

consisting of heterogeneous receivers, this section also develops a phase-only IE-FDMA model. Next, Sect. 3 presents the experimental results, including the network products and user positioning in two networks: one equipped with homogeneous receivers and another equipped with heterogeneous receivers. Finally, Sect. 4 summarizes our findings and presents our conclusions.

2 Methods

This section presents the GLONASS PPP-RTK concept by taking advantage of the IE-FDMA model proposed in Teunissen (2019). We start with the undifferenced and uncombined GNSS observation equations. Next, we revisit the code-plus-phase CDMA PPP-RTK model and extend it to FDMA observables, making it applicable to networks equipped with homogeneous receivers. Subsequently, we consider the case of heterogeneous receivers, for which we derive a phase-only IE-FDMA model. Finally, we end with a discussion.

2.1 Undifferenced and uncombined GNSS code and phase observation equations

We commence with the undifferenced and uncombined GNSS code and phase observation equations of a network receiver r ($r = 1, \dots, n$) that tracks satellite s ($s = 1, \dots, m$) at frequency j ($j = 1, \dots, f$), which can be expressed as (Leick et al. 2015)

$$\begin{aligned} E\left[p^s_{r,j}\right] &= m^s_r \tau_r + \mathrm{d}t_r - \mathrm{d}t^s + \mu_j I^s_r + d^s_{r,j} - d^s_j \\ E\left[\phi^s_{r,j}\right] &= m^s_r \tau_r + \mathrm{d}t_r - \mathrm{d}t^s - \mu_j I^s_r + \delta^s_{r,j} - \delta^s_j + \lambda^s_j z^s_{r,j} \end{aligned} \tag{1}$$

where $E[\cdot]$ denotes the expectation operator and $p^s_{r,j}$ ($\phi^s_{r,j}$) represents the observed-minus-calculated code (phase) observable. Here, we assume that the observed-minus-calculated observables comprise, among others, the receiver-satellite range. The unknowns therefore include the zenith wet tropospheric delay τ_r with its mapping function m^s_r, the receiver (satellite) clock $\mathrm{d}t_r$ ($\mathrm{d}t^s$), the first-order slant ionospheric delay I^s_r linked to multi-frequency observables by the scalar $\mu_j = \left(\lambda^s_j / \lambda^s_1\right)^2$ with λ^s_j being the wavelength, the receiver code (phase) bias $d^s_{r,j}$ ($\delta^s_{r,j}$), the satellite code (phase) bias d^s_j (δ^s_j), and the integer ambiguity $z^s_{r,j}$. We note that the frequency-dependent receiver code and phase biases ($d^s_{r,j}$ and $\delta^s_{r,j}$) are satellite-specific in the GLONASS observation equations since the GLONASS satellites in common view differ in frequency (and wavelength λ^s_j). For CDMA systems, in which all satellites share common frequencies, the wavelength identifier reduces to λ_j, and the receiver biases ($d_{r,j}$ and $\delta_{r,j}$) become satellite-independent.

2.2 Revisiting the CDMA PPP-RTK model

Several PPP-RTK methods exist in the literature (Collins et al. 2010; Ge et al. 2008; Laurichesse et al. 2009; Teunissen et al. 2010; Zhang et al. 2011). For an overview and a critical comparison, see (Teunissen and Khodabandeh 2015). Here, we focus on the undifferenced and uncombined common clock model due to its several benefits (Odijk et al. 2016). The undifferenced and uncombined formulation preserves all original information and enables flexible extension to an arbitrary number of frequencies and systems. The common clock construction parameterizes one receiver clock for both code and phase observables, making the receiver biases estimable; thus, a dynamic model can be imposed to strengthen the model.

We revisit the CDMA PPP-RTK model to explore how we can extend it to the FDMA GLONASS system. Keeping this in mind, we start from Eq. (1), which is a rank-deficient system. One must address the rank deficiencies between some columns of the design matrix and establish a uniquely estimable system. The S-system theory is suitable to carry out this work (Baarda 1973; Teunissen 1985). It first identifies the rank deficiencies and then chooses some parameters as the S-basis (datum) to eliminate the rank deficiencies. Here, we follow the S-basis selected in Odijk et al. (2016), thereby forming the full-rank CDMA PPP-RTK network model as

$$\begin{aligned} E\left[p^s_{r,j}\right] &= m^s_r \tilde{\tau}_r + \mathrm{d}\tilde{t}_r - \mathrm{d}\tilde{t}^s + \mu_j \tilde{I}^s_r + \tilde{d}_{r,j} - \tilde{d}^s_j \\ E\left[\phi^s_{r,j}\right] &= m^s_r \tilde{\tau}_r + \mathrm{d}\tilde{t}_r - \mathrm{d}\tilde{t}^s - \mu_j \tilde{I}^s_r + \tilde{\delta}_{r,j} - \tilde{\delta}^s_j + \lambda_j \tilde{z}^s_{r,j} \end{aligned} \tag{2}$$

where the superscript '~' indicates that the estimable parameters in Eq. (2) are not the original unknowns in Eq. (1) but rather the reparameterized quantities that absorb the S-basis selected. Since Eq. (2) parameterizes the ionospheric delay without external constraints, we refer to the model as the ionosphere-float variant (Odijk et al. 2016). Table 1 provides the interpretations of the estimable parameters.

As shown in Table 1, $d_{r,IF} = \frac{\mu_2}{\mu_2 - \mu_1} d_{r,1} - \frac{\mu_1}{\mu_2 - \mu_1} d_{r,2}$ denotes the ionosphere-free receiver code bias, and $d_{r,GF} = \frac{1}{\mu_2 - \mu_1}\left(d_{r,2} - d_{r,1}\right)$ represents the geometry-free receiver code bias. The ionosphere-free satellite code bias $d^s_{,IF}$ and the geometry-free satellite code bias $d^s_{,GF}$ have the same structures as those of their receiver counterparts. Notably, in regional networks with inter-station distances smaller than 500 km (Rocken et al. 1993), we consider a rank deficiency originating from tropospheric delays and satellite clocks since the tropospheric mapping functions are almost identical for all receivers (Odijk et al. 2016).

Table 1 Estimable parameters of the GNSS code-plus-phase ionosphere-float PPP-RTK model and their interpretations

Estimable parameter	Notation and interpretation
Zenith tropospheric delay	$\tilde{\tau}_r = \tau_r \; \lfloor -\tau_1 \;\; (r > 1) \rfloor$
Receiver clock	$\mathrm{d}\tilde{t}_r = \left(\mathrm{d}t_r + d_{r,IF}\right) - \left(\mathrm{d}t_1 + d_{1,IF}\right) \;\; (r > 1)$
Satellite clock	$\mathrm{d}\tilde{t}^s = \left(\mathrm{d}t^s + d^s_{,IF}\right) - \left(\mathrm{d}t_1 + d_{1,IF}\right) \; \lfloor -m^s_1 \tau_1 \rfloor$
Ionospheric delay	$\tilde{I}^s_r = I^s_r + d_{r,GF} - d^s_{,GF}$
Receiver code bias	$\tilde{d}_{r,j} = \left(d_{r,j} - d_{r,IF} - \mu_j d_{r,GF}\right) - \left(d_{1,j} - d_{1,IF} - \mu_j d_{1,GF}\right) \quad (j > 2, r > 1)$
Satellite code bias	$\tilde{d}^s_{,j} = \left(d^s_{,j} - d^s_{,IF} - \mu_j d^s_{,GF}\right) - \left(d_{1,j} - d_{1,IF} - \mu_j d_{1,GF}\right) \quad (j > 2)$
Receiver phase bias	$\tilde{\delta}_{r,j} = \left(\delta_{r,j} - d_{r,IF} + u_j d_{r,GF}\right) - \left(\delta_{1,j} - d_{1,IF} + u_j d_{1,GF}\right) + \lambda^1_j (z^1_{r,j} - z^1_{1,j}) \quad (r > 1)$
Satellite phase bias	$\tilde{\delta}^s_{,j} = \left(\delta^s_{,j} - d^s_{,IF} + \mu_j d^s_{,GF}\right) - \left(\delta_{1,j} - d_{1,IF} + u_j d_{1,GF}\right) - \lambda^s_j z^s_{1,j}$
Integer ambiguity	$\tilde{z}^s_{r,j} = (z^s_{r,j} - z^s_{1,j}) - (z^1_{r,j} - z^1_{1,j}) \quad (r > 1, s > 1)$ for CDMA $\tilde{z}^s_{r,j} = a_1(z^s_{r,j} - z^s_{1,j}) - a_s(z^1_{r,j} - z^1_{1,j}) \quad (r > 1, s > 1)$ for FDMA

The items in $\lfloor \rfloor$ exist only for regional networks and vanish for large-scale networks

In Table 1, the estimable receiver clock, receiver code and phase biases are not absolute terms but rather relative quantities with respect to receiver 1. Hence, the common biases involved in network receivers can be implicitly eliminated, thereby preventing them from undermining the parameter estimation. This should be kept in mind since some biases in homogeneous receivers indeed present similar characteristics, unexceptionally, the IFB, a nuisance for GLONASS data processing (Reussner and Wanninger 2011; Wanninger 2012).

Equation (2) represents the full-rank CDMA PPP-RTK model on the network side. Providing users with satellite clocks, satellite phase biases (and code biases for $j > 2$) and, optionally, the ionospheric corrections, one can establish the full-rank CDMA PPP-RTK model on the user side. For the sake of brevity, we omit the ionospheric corrections here. Hence, the full-rank CDMA PPP-RTK user model can be written as (Odijk et al. 2016)

$$\begin{aligned} E\left[p^s_{u,j} + \mathrm{d}\tilde{t}^s + \tilde{d}^s_j\right] &= e^s_u \Delta x + m^s_u \tilde{\tau}_u + \mathrm{d}\tilde{t}_u + \mu_j \tilde{I}^s_u + \tilde{d}_{u,j} \\ E\left[\phi^s_{u,j} + \mathrm{d}\tilde{t}^s + \tilde{\delta}^s_j\right] &= e^s_u \Delta x + m^s_u \tilde{\tau}_u + \mathrm{d}\tilde{t}_u - \mu_j \tilde{I}^s_u + \tilde{\delta}_{u,j} + \lambda_j \tilde{z}^s_{u,j} \end{aligned} \tag{3}$$

where the subscript 'u' indicates that the parameters correspond to a user receiver. The observed-minus-calculated observables $p^s_{u,j}$ and $\phi^s_{u,j}$ on the user side exempt the user position, which, on the right side, is parameterized as a three-dimensional unknown vector Δx with its coefficient the line-of-sight vector e^s_u. The definitions of the other unknowns are identical to those in Eq. (2), corresponding to the receiver not selected as a reference ($r > 1$), and can be denoted by referring to those listed in Table 1 and replacing the subscript 'r' ($r > 1$) with 'u'.

Note that Eq. (3) is actually equivalent to Eq. (2) once the satellite clock and satellite bias of Eq. (2) are moved from the right side to the left side and the receiver position is estimated. Thus, the PPP-RTK user can be considered a special network station that estimates its position but loses the contribution to product estimation. The user model also parameterizes the differential receiver biases linked to network receiver 1, implying the elimination of common receiver biases in the process of parameter estimation.

2.3 GLONASS code-plus-phase PPP-RTK model

We now develop the GLONASS FDMA PPP-RTK model. This subsection derives the model extended from the CDMA model, which uses both code and phase observables, namely, the code-plus-phase model. In addition to the ionosphere-float variant, we consider an ionosphere-weighted variant that imposes a weighted constraint on the ionospheric parameters.

2.3.1 Ionosphere-float variant

To develop the GLONASS model, a natural idea is to adopt the same principle underlying the CDMA model while also carefully takes the IFBs into account. This tentative solution proceeds by selecting the same S-basis pertaining to the CDMA model, yielding the reparameterized GLONASS code and phase observation equations as

$$E\left[p_{r,j}^{s}\right] = m_r^s\tilde{\tau}_r + \mathrm{d}\tilde{t}_r^s - \mathrm{d}\tilde{t}^s + \mu_j\tilde{l}_r^s + \tilde{d}_{r,j}^s - \tilde{d}_j^s$$
$$E\left[\phi_{r,j}^{s}\right] = m_r^s\tilde{\tau}_r + \mathrm{d}\tilde{t}_r^s - \mathrm{d}\tilde{t}^s - \mu_j\tilde{l}_r^s + \tilde{\delta}_{r,j}^s - \tilde{\delta}_j^s + \left(\lambda_j^s\bar{z}_{r,j}^s - \lambda_j^1\bar{z}_{r,j}^1\right) \quad (4)$$

where the receiver clock $\mathrm{d}\tilde{t}_r^s$, receiver biases $\tilde{d}_{r,j}^s$ and $\tilde{\delta}_{r,j}^s$ are now satellite-specific. The receiver clock is satellite-specific because it absorbs the code biases. $\bar{z}_{r,j}^s = z_{r,j}^s - z_{1,j}^s$ is the between-receiver single-differenced ambiguity.

Equation (4) is still rank deficient due to the additional parameters arising from the IFB. The size of the rank deficiency originating from $\tilde{\delta}_{r,j}^s$ and $\bar{z}_{r,j}^s$ is exactly the number of $\bar{z}_{r,j}^s$, resulting in the nonexistence of estimable integer ambiguities once we choose $\bar{z}_{r,j}^s$ as the S-basis. Thus, the integer property of ambiguities is impossible to recover when parameterizing satellite-specific GLONASS receiver biases. One way to overcome this problem is to calibrate the code and phase IFBs beforehand. However, a GLONASS IFB look-up table consisting of all receiver types requires massive work. When considering an alternative method, one question is whether the IFB can be ignored. Fortunately, the answer is in the affirmative as long as the network is equipped with homogeneous receivers. Since the IFBs in this case are virtually the same (Reussner and Wanninger 2011; Wanninger 2012), the between-receiver single-differenced terms parameterized in Eq. (4) are free of IFBs. As an example, we provide insights into how IFBs are eliminated in the estimable receiver clock. Assuming that IFBs are identical in homogeneous receivers, we can separate the original GLONASS receiver code bias into a receiver-dependent bias and a satellite-dependent term (Reussner and Wanninger 2011)

$$d_{r,j}^s = d_{r,j} + \gamma_j^s \quad (5)$$

where γ_j^s denotes the bias for satellite s.

Inserting Eq. (5) into the estimable receiver clock yields

$$\begin{aligned}\mathrm{d}\tilde{t}_r^s &= \left(\mathrm{d}t_r + d_{r,IF}^s\right) - \left(\mathrm{d}t_1 + d_{1,IF}^s\right)\ (r>1)\\ &= \left(\mathrm{d}t_r + d_{r,IF} + \gamma_{,IF}^s\right) - \left(\mathrm{d}t_1 + d_{1,IF} + \gamma_{,IF}^s\right)\ (r>1)\\ &= \mathrm{d}\tilde{t}_r\ (r>1)\end{aligned} \quad (6)$$

where we see that the common ionosphere-free satellite-dependent biases $\gamma_{,IF}^s$ between two receivers are eliminated. Finally, the GLONASS estimable receiver clock $\mathrm{d}\tilde{t}_r^s$ reduces to the satellite-independent unknown $\mathrm{d}\tilde{t}_r$. Along a similar line, the receiver code and phase biases reduce to $\tilde{d}_{r,j}$ and $\tilde{\delta}_{r,j}$, reforming the GLONASS observation equations as

$$E\left[p_{r,j}^{s}\right] = m_r^s\tilde{\tau}_r + \mathrm{d}\tilde{t}_r - \mathrm{d}\tilde{t}^s + \mu_j\tilde{l}_r^s + \tilde{d}_{r,j} - \tilde{d}_j^s$$
$$E\left[\phi_{r,j}^{s}\right] = m_r^s\tilde{\tau}_r + \mathrm{d}\tilde{t}_r - \mathrm{d}\tilde{t}^s - \mu_j\tilde{l}_r^s + \tilde{\delta}_{r,j} - \tilde{\delta}_j^s + \left(\lambda_j^s\bar{z}_{r,j}^s - \lambda_j^1\bar{z}_{r,j}^1\right) \quad (7)$$

where the ambiguities are still inestimable.

To construct estimable ambiguities, we follow the formulation proposed in Teunissen (2019). Then, the estimable (full-rank) GLONASS code-plus-phase model can be written as

$$E\left[p_{r,j}^{s}\right] = m_r^s\tilde{\tau}_r + \mathrm{d}\tilde{t}_r - \mathrm{d}\tilde{t}^s + \mu_j\tilde{l}_r^s + \tilde{d}_{r,j} - \tilde{d}_j^s$$
$$E\left[\phi_{r,j}^{s}\right] = m_r^s\tilde{\tau}_r + \mathrm{d}\tilde{t}_r - \mathrm{d}\tilde{t}^s - \mu_j\tilde{l}_r^s + \tilde{\delta}_{r,j} - \tilde{\delta}_j^s + \frac{2848\lambda_j}{a_1 a_s}\tilde{z}_{r,j}^s \quad (8)$$

where $a_s = 2848 + \kappa^s$ with $\kappa^s \in [-7, +6]$ being the channel number of the GLONASS satellite; λ_j is the wavelength of the center frequency L1 or L2 with $\kappa^s = 0$; and $\tilde{z}_{r,j}^s = a_1(z_{r,j}^s - z_{1,j}^s) - a_s(z_{r,j}^1 - z_{1,j}^1)$ is the estimable GLONASS ambiguity, which is not the standard double-differenced ambiguity but a linear combination of original ambiguities. Note that herein, only the GLONASS L1 + L2 case is considered since the GLONASS L3 signal adopts CDMA modulation.

The ambiguities in Eq. (8) are, however, still not ready for integer ambiguity resolution since fixing $\tilde{z}_{r,j}^s$ as integers is not sufficient to ensure the integer property of the original undifferenced ambiguities. To conduct rigorous integer ambiguity resolution, we must transform the estimable ambiguities into integer-estimable ambiguities (Teunissen 2019). We now rewrite the estimable ambiguities together with their coefficients in Eq. (8) in compact form as $(\Lambda \otimes H')\tilde{Z}_r$ $(r>1)$, in which $\tilde{Z}_r = [\tilde{Z}_{r,1}, \tilde{Z}_{r,2}]^T \in \mathbb{Z}^{2(m-1)}$ is the estimable ambiguity vector with $\tilde{Z}_{r,j} = [\tilde{z}_{r,j}^2, \ldots, \tilde{z}_{r,j}^m]$, $\Lambda = diag(\lambda_1, \lambda_2)$ is the diagonal matrix of wavelengths, and $H' = diag(\frac{2848}{a_1 a_2}, \ldots, \frac{2848}{a_1 a_m})$. As proposed in Teunissen (2019), the integer-estimable ambiguities, together with their coefficients, are defined as $(\Lambda \otimes L)\hat{Z}_r$ $(r>1)$. Here, for brevity, we omit the analytical forms of $\hat{Z}_r$ and L, which can be found in Teunissen (2019).

Finally, we obtain the GLONASS IE-FDMA code-plus-phase network model by replacing the estimable ambiguities $(\Lambda \otimes H')\tilde{Z}_r$ with the integer-estimable ones $(\Lambda \otimes L)\hat{Z}_r$, to which rigorous integer ambiguity resolution is readily applicable. Along a similar line, one can obtain the user model by replacing the CDMA ambiguities in Eq. (3) with the GLONASS integer-estimable ambiguities of a user receiver $(\Lambda \otimes L)\hat{Z}_u$.

2.3.2 Ionosphere-weighted variant

Instead of parameterizing the ionospheric delay without any a priori information, the ionosphere-weighted variant imposes a weighted constraint on between-receiver single-differenced ionospheric delays, which strengthens the model. Experience in deriving the ionosphere-float variant indicates that we can extend the CDMA model to FDMA observables by simply replacing the CDMA ambiguities with the FDMA ambiguities. Here, we employ the CDMA ionosphere-weighted PPP-RTK variant in Odijk et al. (2016) and extend it to FDMA signals as follows:

$$\begin{aligned} E\left[p^s_{r,j}\right] &= m^s_r\tilde{\tau}_r + \mathrm{d}\tilde{t}_r - \mathrm{d}\tilde{t}^s + \mu_j\tilde{\tilde{l}}^s_r + \mu_j\tilde{d}_{r,GF} + \tilde{d}_{r,j} - \tilde{d}^s_{,j} \\ E\left[\phi^s_{r,j}\right] &= m^s_r\tilde{\tau}_r + \mathrm{d}\tilde{t}_r - \mathrm{d}\tilde{t}^s - \mu_j\tilde{\tilde{l}}^s_r + \tilde{\tilde{\delta}}_{r,j} - \tilde{\delta}^s_{,j} + \frac{2848\lambda_j}{a_1 a_s}\tilde{z}^s_{r,j} \\ E\left[-l^s_1 + l^s_r\right] &= -\tilde{\tilde{l}}^s_1 + \tilde{\tilde{l}}^s_r \end{aligned} \tag{9}$$

where $-l^s_1 + l^s_r$ is the between-receiver single-differenced pseudo-observable, which is commonly set as zero in practice for a regional network (Teunissen 1998). The superscript '$\tilde{\cdot}$' indicates that the definitions of the estimable ionospheric delay and receiver phase bias differ from those estimated in the ionosphere-float variant case. We also note that the ionosphere-weighted variant estimates the differential code bias $\tilde{d}_{r,GF}$. Table 2 lists the interpretations of these new parameters, while the same unknowns as those in the ionosphere-float variant case are defined in Table 1.

Similarly, for a rigorous integer ambiguity resolution, we transform the estimable ambiguities in Eq. (9) into integer-estimable ones $(\Lambda \otimes L)\hat{Z}_r$, thereby yielding the IE-FDMA ionosphere-weighted network model.

The ionosphere-weighted user model employs not only satellite clocks and satellite biases but also ionospheric corrections. We generate the user-specific ionospheric correction $l^s_{u,cor}$ by using the Kriging interpolation technique (Odijk 2002). After these corrections are implemented, the estimable ionosphere-weighted user model can be written as

$$\begin{aligned} E\left[p^s_{u,j} + \mathrm{d}\tilde{t}^s + \tilde{d}^s_{,j}\right] &= e^s_u\Delta x + m^s_u\tilde{\tau}_u + \mathrm{d}\tilde{t}_u + \mu_j\tilde{\tilde{l}}^s_u + \mu_j\tilde{d}_{u,GF} + \tilde{d}_{u,j} \\ E\left[\phi^s_{u,j} + \mathrm{d}\tilde{t}^s + \tilde{\delta}^s_{,j}\right] &= e^s_u\Delta x + m^s_u\tilde{\tau}_u + \mathrm{d}\tilde{t}_u - \mu_j\tilde{\tilde{l}}^s_u + \tilde{\tilde{\delta}}_{u,j} + \frac{2848\lambda_j}{a_1 a_s}\tilde{z}^s_{u,j} \\ E\left[l^s_{u,cor}\right] &= \tilde{\tilde{l}}^s_u \end{aligned} \tag{10}$$

from which we can develop the IE-FDMA model by replacing the estimable ambiguities with integer-estimable ambiguities $(\Lambda \otimes L)\hat{Z}_u$.

Table 2 Estimable parameters of the GNSS code-plus-phase ionosphere-weighted PPP-RTK model and their interpretations

Estimable parameter	Notation and interpretation
Ionospheric delay	$\tilde{\tilde{l}}^s_r = l^s_r + d_{1,GF} - d^s_{,GF}$
Receiver differential code bias	$\tilde{d}_{r,GF} = d_{r,GF} - d_{1,GF} \quad (r > 1)$
Receiver phase bias	$\tilde{\tilde{\delta}}_{r,j} = (\delta_{r,j} - d_{r,IF}) - (\delta_{1,j} - d_{1,IF}) + \lambda^1_j(z^1_{r,j} - z^1_{1,j}) \quad (r > 1)$

Note that here, we list only the parameters different from those of the ionosphere-float model. Concerning the remaining parameters, see Table 1

2.4 GLONASS phase-only PPP-RTK model

The code-plus-phase model derived above establishes a unified framework of GNSS PPP-RTK for both CDMA and FDMA systems but is limited to a network equipped with homogeneous receivers. This section considers the more general case where the receivers in the network are heterogeneous. To circumvent the code IFBs that occur in heterogeneous receivers, we exclude the GLONASS code observables and utilize only the phase observables, forming the so-called phase-only model. The integer-estimability underlying the phase-only ionosphere-float RTK model was proposed in Teunissen (2019); here, we extend it to PPP-RTK and consider the ionosphere-weighted variant.

2.4.1 Ionosphere-float variant

Starting from the GLONASS phase observation equation in Eq. (1), we first derive the ionosphere-float variant. Since we exclude the code observables, the rank deficiencies must be reidentified and then eliminated in a step-by-step manner. Four types of rank deficiency can be easily identified since exclusion of code observables has no impact on them: (1) rank deficiency of size 1 between receiver and satellite clocks, (2) rank deficiency of size *fn* between receiver phase biases and ambiguities, (3) rank deficiency of size *fm* between satellite phase biases and ambiguities, and (4) rank deficiency of size 1 between tropospheric delays and satellite clocks (for regional networks only). We select, following the idea underlying the code-plus-phase model, $\mathrm{d}t_1$, $z^1_{r\neq 1,j}$, $\delta_{1,j}$, $z^s_{1,j}$ and τ_1 as the S-basis to eliminate the rank deficiencies. After reparameterization, the phase observation equation can be written as

$$E\left[\phi^s_{r,j}\right] = m^s_r\tilde{\tau}_r + \mathrm{d}\bar{t}_r - \mathrm{d}\bar{t}^s - \mu_j l^s_r + \bar{\delta}_{r,j} - \bar{\delta}^s_{,j} + \frac{2848\lambda_j}{a_1 a_s}\tilde{z}^s_{r,j} \tag{11}$$

where the ambiguity is now the same as that in the code-plus-phase model, namely, a specific combination of original ambiguities. The reparameterized tropospheric delay $\tilde{\tau}_r$ is defined in Table 1. The parameters identified by '–' are no

longer the original unknowns but instead include the S-basis selected. Their analytical expressions are

$$\begin{aligned}
&\bar{\mathrm{d}t}_r = \left(\mathrm{d}t_r - \mathrm{d}t_1\right) \ (r>1)\\
&\bar{\mathrm{d}t}^s = \mathrm{d}t^s - dt_1 \ \lfloor -m_1^s\tau_1 \rfloor\\
&\bar{\delta}_{r,j} = \delta_{r,j} - \delta_{1,j} + \lambda_j^1\left(z_{r,j}^1 - z_{1,j}^1\right) \ (r>1)\\
&\bar{\delta}_{,j}^s = \delta_{,j}^s - \delta_{1,j} - \lambda_j^s z_{1,j}^s
\end{aligned} \tag{12}$$

where the reparameterized receiver phase bias $\bar{\delta}_{r,j}$ is independent of the satellite, implying the ignorance of between-receiver single-differenced phase IFB, which is permitted since this term is small enough in most practical cases (Sleewagen 2012). $\lfloor -m_1^s\tau_1 \rfloor$ exists only for regional networks with inter-station distances smaller than 500 km and vanishes in networks with a larger scale.

The code-plus-phase model developed earlier shows that the column of the design matrix for code biases is linearly correlated to those for clocks and ionospheric delays. Equation (11) encounters similar linear correlations between the phase biases, clocks, and ionospheric delays, resulting in four other types of rank deficiencies between: (1) receiver phase biases and receiver clocks of size $n-1$; (2) receiver phase biases and ionospheric delays of size $n-1$; (3) satellite phase biases and satellite clocks of size m; and (4) satellite phase biases and ionospheric delays of size m. We select $\bar{\delta}_{r>1,j=1,2}$ and $\bar{\delta}_{,j=1,2}^s$ as the S-basis to eliminate the rank deficiencies, generating the equation

$$E\left[\phi_{r,j}^s\right] = m_r^s\tilde{\tau}_r + \bar{\mathrm{d}t}_r - \bar{\mathrm{d}t}^s - \mu_j\bar{l}_r^s + \frac{2848\lambda_j}{a_1 a_s}\tilde{z}_{r,j}^s \tag{13}$$

where the definitions of the reparameterized unknowns are

$$\begin{aligned}
&\bar{\mathrm{d}t}_r = \mathrm{d}t_r + \bar{\delta}_{r,IF} \ (r>1)\\
&\bar{\mathrm{d}t}^s = \mathrm{d}t^s + \bar{\delta}_{,IF}^s\\
&\bar{l}_r^s = l_r^s - \bar{\delta}_{,GF}^s + \bar{\delta}_{r,GF}
\end{aligned} \tag{14}$$

where the structures of the geometry-free and ionosphere-free combination of the phase bias resemble those of the code bias defined earlier.

The last type of rank deficiency stems from ionospheric delays and ambiguities, whose size is $(m-1)(n-1)$, for which we select the ambiguities at the first frequency $\tilde{z}_{r\neq1,j=1}^{s\neq1}$ as the S-basis to eliminate. The full-rank GLONASS phase-only network PPP-RTK model is finally formulated as

$$E\left[\phi_{r,j}^s\right] = m_r^s\tilde{\tau}_r + \bar{\mathrm{d}t}_r - \bar{\mathrm{d}t}^s - \mu_j\bar{\bar{l}}_r^s + \frac{2848\lambda_2}{7a_1a_s}\bar{\bar{z}}_{r,2}^s \tag{15}$$

where the estimable ionospheric delay and ambiguity are

$$\begin{aligned}
&\bar{\bar{l}}_r^s = \bar{l}_r^s - \frac{2848\lambda_1}{a_1a_s}\tilde{z}_{r,1}^s\\
&\bar{\bar{z}}_{r,2}^s = 7\tilde{z}_{r,2}^s - 9\tilde{z}_{r,1}^s \ (j=2)
\end{aligned} \tag{16}$$

where the coefficients 7 and 9 originate from the fact that $\lambda_1/\lambda_2 = 7/9$, the ambiguities exist only at frequency 2, and the phase biases are no longer estimable but absorbed into the other parameters. Considering the IE-FDMA model, we replace the estimable ambiguities with the integer-estimable ambiguities $\frac{\lambda_2 L}{7}\left(7\hat{Z}_{r,2} - 9\hat{Z}_{r,1}\right)$, of which the analytical forms of $\hat{Z}_{r,1}$ and $\hat{Z}_{r,2}$ are given in (Teunissen 2019). Table 3 lists the notations and interpretations of the estimable parameters.

On the user side, only the satellite clocks are provided, yielding the estimable user model

Table 3 Estimable parameters of the GLONASS phase-only ionosphere-float PPP-RTK model and their interpretations

Estimable parameter	Notation and interpretation
Tropospheric delay	$\tilde{\tau}_r = \tau_r \ \lfloor -\tau_1 \ (r>1) \rfloor$
Receiver clock	$\bar{\bar{\mathrm{d}t}}_r = \mathrm{d}t_r - \mathrm{d}t_1 + \delta_{r,IF} - \delta_{1,IF} + \left(\lambda^1 z_{r,}^1\right)_{IF} - \left(\lambda^1 z_{1,}^1\right)_{IF} \quad (r>1)$
Satellite clock	$\bar{\bar{\mathrm{d}t}}^s = \mathrm{d}t^s - \mathrm{d}t_1 + \delta_{,IF}^s - \delta_{1,IF} - \left(\lambda^s z_{1,}^s\right)_{IF} \lfloor -m_1^s\tau_1 \rfloor$
Ionospheric delay	$\bar{\bar{l}}_r^s = l_r^s - \delta_{,GF}^s + \delta_{1,GF} + \left(\lambda^s z_{1,}^s\right)_{GF} + \delta_{r,GF} - \delta_{1,GF} + \left(\lambda^1 z_{r,}^1\right)_{GF} - (\lambda^1 z_{1,}^1)_{GF} - \lambda_1^s(z_{r,1}^s - z_{1,1}^s) + \lambda_1^1(z_{r,1}^1 - z_{1,1}^1)$
Ambiguity	$\bar{\bar{z}}_{r,2}^s = 7\left[a_1(z_{r,2}^s - z_{1,2}^s) - a_s(z_{r,2}^1 - z_{1,2}^1)\right] - 9\left[a_1(z_{r,1}^s - z_{1,1}^s) - a_s(z_{r,1}^1 - z_{1,1}^1)\right] \quad (j=2)$

The items in $\sqcup$ exist only for regional networks and vanish for large-scale networks

$$E\left[\phi^s_{u,j} + \mathrm{d}\bar{\bar{t}}^s\right] = e^s_u \Delta x + m^s_u \tilde{\tau}_u + \mathrm{d}\bar{\bar{t}}_u - \mu_j \bar{\bar{l}}^s_u + \frac{2848\lambda_2}{7a_1a_s}\bar{\bar{z}}^s_{u,2} \tag{17}$$

where we note that replacing the estimable ambiguities with $\frac{\lambda_2 L}{7}\left(7\hat{Z}_{u,2} - 9\hat{Z}_{u,1}\right)$ finally generates the IE-FDMA user model.

2.4.2 Ionosphere-weighted variant

The derivation of the ionosphere-weighted variant proceeds along a similar line as that in the case of the ionosphere-float variant, which is tractable once we recognize that the rank deficiencies involved in the two models are the same except for two types related to ionospheric delays. One type of rank deficiency originates from the ionospheric delays and receiver phase biases, while the other type stems from the ionospheric delays and ambiguities. Both can be removed in the case of the ionosphere-weighted variant due to the introduction of ionospheric pseudo-observables. We eliminate the remaining rank deficiencies by selecting the same S-basis underlying the ionosphere-float variant. Therefore, the estimable GLONASS phase-only ionosphere-weighted network PPP-RTK model can be written as

$$\begin{aligned} E\left[\phi^s_{r,j}\right] &= m^s_r \tilde{\tau}_r + \mathrm{d}\hat{t}_r - \mathrm{d}\bar{\bar{t}}^s - \mu_j \hat{l}^s_r + \hat{\delta}_{r,j} + \frac{2848\lambda_j}{a_1 a_s}\tilde{z}^s_{r,j} \\ E\left[-l^s_1 + l^s_r\right] &= -\hat{l}^s_1 + \hat{l}^s_r \end{aligned} \tag{18}$$

where the estimable parameters denoted by '$\hat{\cdot}$' and ambiguities differ from those in the ionosphere-float variant case; see Table 4. The other estimable parameters are the same as those defined in Table 3. Since the estimable ambiguities are identical to those in the code-plus-phase model, the ambiguities constructed in the IE-FDMA model are $(\Lambda \otimes L)\hat{Z}_r$.

Finally, we provide users with satellite clocks and ionospheric corrections, forming the user model

$$\begin{aligned} E\left[\phi^s_{u,j} + \mathrm{d}\bar{\bar{t}}^s\right] &= e^s_u \Delta x + m^s_u \tilde{\tau}_u + \mathrm{d}\hat{t}_u - \mu_j \hat{l}^s_u + \hat{\delta}_{u,j} + \frac{2848\lambda_j}{a_1 a_s}\tilde{z}^s_{u,j} \\ E\left[l^s_{u,cor}\right] &= \hat{l}^s_u \end{aligned} \tag{19}$$

from which the IE-FDMA user model can be developed by replacing the estimable ambiguities with $(\Lambda \otimes L)\hat{Z}_u$.

2.5 Discussion

In brief, Eqs. (8) and (9), respectively, denote the estimable (full-rank) GLONASS code-plus-phase ionosphere-float and ionosphere-weighted PPP-RTK models, while Eqs. (15) and (18), respectively, represent the estimable GLONASS phase-only ionosphere-float and ionosphere-weighted PPP-RTK models. To obtain the IE-FDMA model, which enables rigorous integer ambiguity resolution, one can just replace the estimable ambiguities in these equations with the integer-estimable ones. Table 5 provides an overview of the models

Table 4 Estimable parameters of the GLONASS phase-only ionosphere-weighted PPP-RTK model and their interpretations

Estimable parameter	Notation and interpretation
Receiver clock	$\mathrm{d}\hat{t}_r = \mathrm{d}t_r - \mathrm{d}t_1 + \delta_{r,1} - \delta_{1,1} + \lambda^1_1(z^1_{r,1} - z^1_{1,1}) \quad (r > 1)$
Ionospheric delay	$\hat{l}^s_r = l^s_r - \delta^s_{,GF} + \delta_{1,GF} + \left(\lambda^s z^s_{1,}\right)_{GF}$
Receiver phase bias	$\hat{\delta}_{r,j} = \delta_{r,j} - \delta_{1,j} + \lambda^1_j(z^1_{r,j} - z^1_{1,j}) - \delta_{r,1} + \delta_{1,1} - \lambda^1_1(z^1_{r,1} - z^1_{1,1}) \quad (r > 1, j > 1)$
Ambiguity	$\tilde{z}^s_{r,j} = a_1(z^s_{r,j} - z^s_{1,j}) - a_s(z^1_{r,j} - z^1_{1,j})$

Note that here, we list only the parameters different from those of the ionosphere-float model. Concerning the remaining parameters, see Table 3

Table 5 An overview of the GLONASS PPP-RTK network models developed in this study

Model	Variant	Full-rank equations	S-basis selected
Code-plus-phase	Ionosphere-float	(8)	$A, d_{r\neq 1,GF}$
	Ionosphere-weighted	(9)	$\underbrace{\lfloor\tau_1\rfloor, \mathrm{d}t_1, d_{r,IF}, d_{1,GF}, d^s_{,IF}, d^s_{,GF}, \delta_{1,j}, z^s_{1,j}, z^1_{r\neq 1,j}}_{A}$
Phase-only	Ionosphere-float	(15)	$B, \delta_{r\neq 1,j=2}, z^{s\neq 1}_{r\neq 1,j=1}$
	Ionosphere-weighted	(18)	$\underbrace{\lfloor\tau_1\rfloor, \mathrm{d}t_1, \delta_{r,j=1}, \delta_{1,j=2}, \delta^s_{,j=1,2}, z^s_{1,j}, z^1_{r\neq 1,j}}_{B}$

The items in $\sqcup$ exist only for regional networks and vanish for large-scale networks

developed in this section. We discuss each model in more detail below.

The code-plus-phase model is applicable to networks equipped with homogeneous receivers. The model is free of external IFB calibration since both code and phase IFBs are implicitly eliminated through reparameterization. We see that the receiver biases involved in receiver 1 are selected as the S-basis, thus forming estimable differential biases. The ionosphere-weighted variant imposes external ionospheric constraints, resulting in a stronger model than the ionosphere-float variant in a regional network. With increasing uncertainty of the ionospheric constraints in a large-scale network, the ionosphere-weighted variant simply converges to the ionosphere-float variant.

The phase-only model enables GLONASS PPP-RTK across heterogeneous receivers. This model utilizes only the phase observables to circumvent the effects of code IFBs. Concerning the phase IFBs, it parameterizes the receiver differential phase biases to carry out implicit elimination, which is reasonable since the differential phase IFBs are small enough to be neglected in most practical cases (Sleewagen 2012). The exclusion of code observables makes the model weaker than the code-plus-phase model, especially for the ionosphere-float variant. The ionosphere-float variant has to select the ambiguities at the first frequency as the S-basis to eliminate the rank deficiencies, resulting in a more difficult situation in terms of integer ambiguity resolution. Fortunately, the weakness of the phase-only model can be remedied by introducing CDMA observables (Teunissen 2019).

3 Results

This section provides the experimental results of GLONASS PPP-RTK based on the models developed earlier. We first introduce the collected data and our processing strategy. Next, we assess the network products and user positioning in two networks.

3.1 Data and processing strategy

To test the code-plus-phase and phase-only models, we selected two regional networks from the National Geodetic Survey (NGS) CORS in the USA. As shown in Fig. 1, the first network (network 1) arranges 20 Leica receivers, of which 8 receivers (red circles) play the role of the network and 12 receivers (blue circles) operate as users. The second network (network 2) deploys, in addition to 8 Leica receivers (3 network receivers and 5 user receivers), 10 Trimble receivers to act as 5 network (red triangles) and 5 user (blue triangles) roles. Table 6 provides the main characteristics of these receivers in the two networks. Since 17 of the 20 stations in network 1 are equipped with the same types of receivers and antennas and the other three come from the same company, it is reasonable to test the code-plus-phase model in this network. For the phase-only model, network 2, equipped with nine different groups of receivers, is suitable to assess its performance. The scales of the two networks are similar, where the inter-station distances, namely the distances between adjacent receivers, range from 40 to 110 km. Both networks track dual-frequency GPS and GLONASS observations with a 30-s sampling interval. The data collection of network 1 commenced on day 001 of 2019 and continued for five days until day 005 of 2019. During this period, some receivers in network 2 missed the GLONASS data; thus, we collected data of network 2 from days 356 to 360 in 2019, when the ionospheric disturbance was as mild as that in the first five days of 2019.

On the network side, we processed the combined GPS and GLONASS data using a Kalman filter. Table 7 provides the detailed data processing strategy. The zenith-referenced standard deviations (STDs) of the code and phase observations for both GPS and GLONASS were set as 0.3 m and

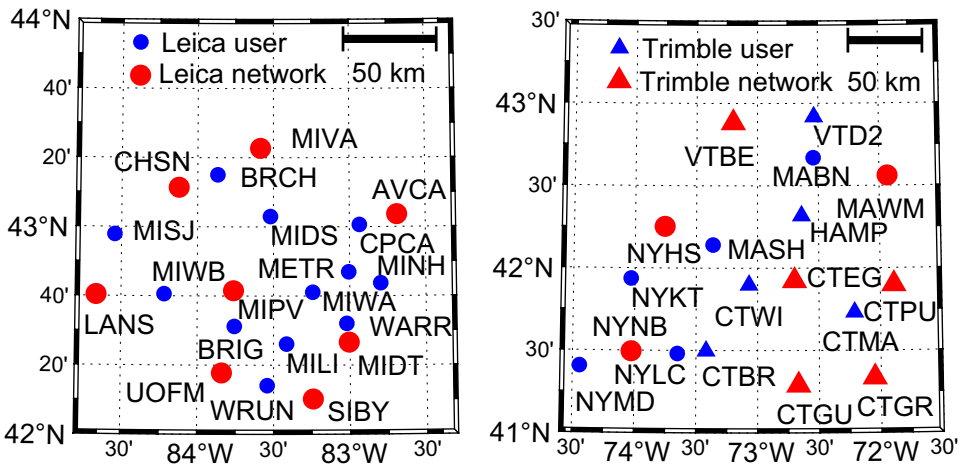

Fig. 1 Station distribution of the network 1 (homogeneous, left hand panel) and network 2 (heterogeneous, right hand panel). The circles represent stations equipped with Leica receivers, while the triangles denote stations equipped with Trimble receivers. Stations marked in red constitute the network reference stations, while the other stations marked in blue act as users

Table 6 Main characteristics of the receivers equipped in the two networks considered

	Receiver	Antenna	Number
Network 1	LEICA GRX1200 + GNSS 9.20/6.405	LEIAT504 LEIS	17
		LEIAR20 LEIM	1
		LEIAT504GG LEIS	1
	LEICA GR50 4.31/7.403	LEIAT504 LEIS	1
Network 2	LEICA GRX1200 + GNSS 9.20/6.405	LEIAR10 NONE	2
	LEICA GR30 4.31/7.403	LEIAR10 NONE	2
		LEIAR20 LEIM	3
	LEICA GR10 4.31/6.525	LEIAR10 NONE	1
	TRIMBLE ALLOY 5.37	TRM57971.00 NONE	6
	TRIMBLE NETR5 48.01	TRM55971.00 NONE	1
	TRIMBLE NETR5 4.48	TRM57971.00 NONE	1
	TRIMBLE NETR9 5.03	TRM57971.00 NONE	1
	TRIMBLE NETR9 5.37	TRM55971.00 NONE	1

Table 7 Data processing strategy adopted in this study for both of GPS and GPS + GLONASS

Item	Strategy
Cutoff elevation angle	10 degrees
Stochastic model	Code/phase zenith STD: 0.3 m/0.003 m; Elevation-dependent weighting by the sine function
Ionospheric delay	White noise estimation
Satellite/receiver clock	
Satellite/receiver bias	Time-constant
Ambiguity	Time-constant in a continuous arc; Cycle slip detection: TurboEdit method (Blewitt 1990)
Tropospheric delay	Dry component: UNB3m model (Leandro et al. 2006) Wet component: random-walk estimation with a spectral density of 0.1 mm/$\sqrt{30}$ s

0.003 m, respectively. Considering the elevation-dependent precision of observations, we adopted the sine weighted function and set the cutoff elevation angle as 10 degrees. For the between-receiver single-differenced ionospheric pseudo-observations, we followed the weighting scheme in Wang et al. (2017), which properly considers the spatial correlation of ionospheric delays. For the parameter estimation, we modeled the clocks and ionospheric delays as white noise, while the code and phase biases were considered as time-constants. The ambiguities were also treated as time-constants unless cycle slips occurred, for which we used the TurboEdit method for detection (Blewitt 1990). Once a cycle slip occurred, we did not repair it but reinitiated the state vector of ambiguities. Regarding the tropospheric delay, the dry component was corrected by the well-known UNB3m model (Leandro et al. 2006), while the zenith wet component was estimated by the random-walk process with a spectral density of 0.1 mm/$\sqrt{30}$ s.

On the user side, the stochastic model and dynamic model were in line with those on the network side. The uncertainty of the corrections was modeled by their variance matrix generated from the network side, and the correlation between corrections was considered. The estimated parameters included, among others, the position components, which were considered unlinked in time. We reinitiated the filter every day to analyze the whole-day positioning performance. We then reprocessed the data by reinitiating the filter every four hours to further analyze the convergence behavior. After obtaining the float solutions, we fixed the integer ambiguities by means of the LAMBDA method (Teunissen 1995). Note that for GLONASS ambiguities, we fixed per frequency only the $m-2$ best-determined ambiguities instead of all $m-1$ ambiguities (Teunissen and Khodabandeh 2019). The core functions of the GPS + GLONASS PPP-RTK software package, including the generation of network products and user positioning, were developed by the second author. Some basic functions, such as file reading and error correction, were provided by the open-source software RTKLIB (Takasu and Yasuda 2009).

3.2 Network equipped with homogeneous receivers

This section aims to test the GLONASS code-plus-phase PPP-RTK model by using the data collected from the

network equipped with homogeneous receivers. We first analyze the quality of network corrections and then present the user positioning results.

3.2.1 Network products

Products estimated on the network side include satellite clocks, satellite phase biases, and ionospheric delays. To provide insights into the characteristics of these corrections, we show the time series of the individual PPP-RTK corrections together with their formal STDs. More importantly, we substantiate, from the experimental perspective, the idea that the precision of combined corrections should also be used for performance evaluation, not only the precision of individual corrections, as theoretically demonstrated in Khodabandeh and Teunissen (2015).

Figure 2 shows the GPS and GLONASS satellite clocks together with their formal STDs estimated by the code-plus-phase ionosphere-float model on day 001 of 2019. The top two panels depict satellites G01 and R01 as examples, showing that both the GPS and GLONASS satellite clocks bear a linear trend. The middle two panels indicate that clocks of different satellites vary in magnitude. What most concerns the PPP-RTK users is the precision of the estimated clocks. As shown in the two bottom panels, the formal STDs of GPS and GLONASS clocks require a period of more than one hour to reach centimeter level, and their final precision is close to two centimeters, which is larger than the precision of phase observations. Does this outcome mean that the estimated satellite clocks are not qualified for the correction of phase observations on the user side? On the other hand, once a new satellite rises, a reinitialization process is needed. Does this mean that the satellite clocks estimated in the reinitialization period are unusable? The answers to these two questions are both negative; we will offer an explanation after analyzing the other two corrections, namely, the satellite phase biases and ionospheric delays.

We now focus on the satellite phase biases, which are critical for recovering the integer property of ambiguities on the user side. As shown in Fig. 3, both the GPS and GLONASS satellite phase biases are stable after initialization. Although the precision of the satellite phase biases increases to some extent when long time-span observations are accumulated, it is still not comparable to the precision of the phase observations. Similar to the satellite clock encounters, the phase bias also undergoes reinitialization when a new satellite rises.

For PPP-RTK users adopting the ionosphere-weighted variant, the ionospheric product is also essential. Figure 4 shows the estimated slant ionospheric delays together with their formal STDs at station BRCH on day 001 of 2019. We see that the time series of both GPS and GLONASS slant ionospheric delays present a '*U*' shape, which is related to the change in elevation angles when satellites pass through the sky over the station. Considering the time series of STDs, the tendency of which is similar to

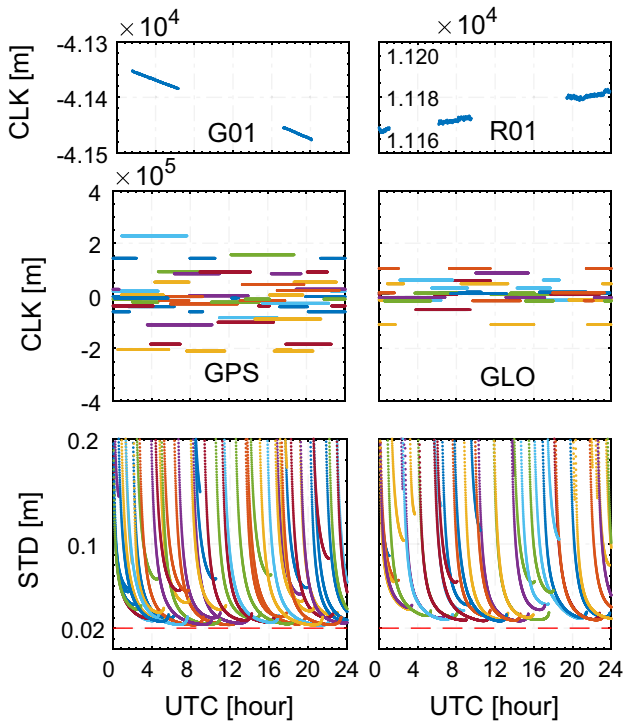

Fig. 2 GPS and GLONASS (GLO) satellite clocks (CLK) together with their formal STDs estimated by the code-plus-phase ionosphere-float model using the data from the network of homogeneous receivers on day 001 of 2019

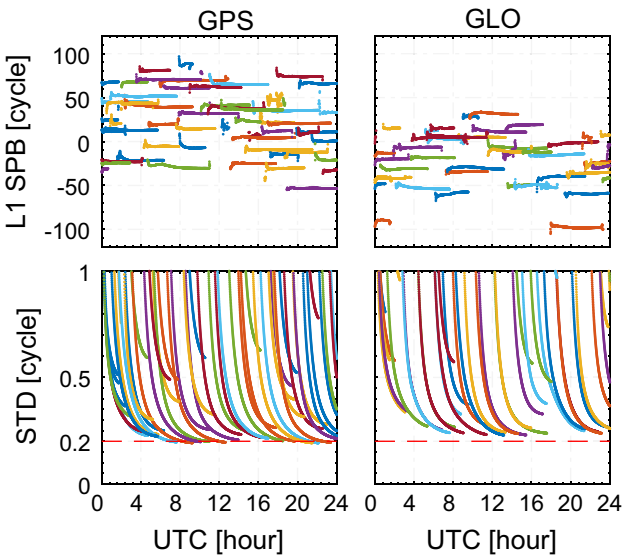

Fig. 3 GPS and GLONASS L1 satellite phase biases (SPBs) together with their formal STDs estimated by the code-plus-phase ionosphere-float model using the data from the network of homogeneous receivers on day 001 of 2019

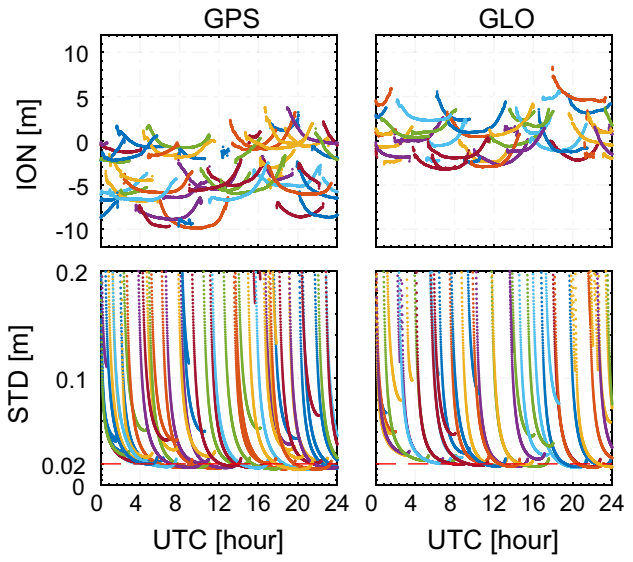

Fig. 4 GPS and GLONASS slant ionospheric (ION) delays at station BRCH together with their formal STDs estimated by the code-plus-phase ionosphere-weighted model using the data from the network of homogeneous receivers on day 001 of 2019

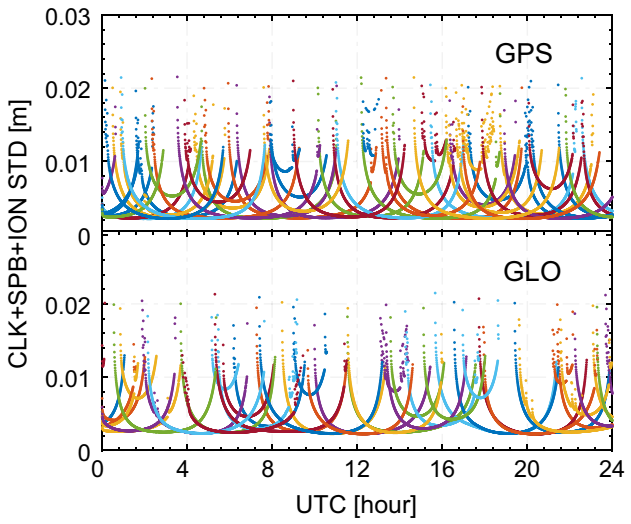

Fig. 5 Formal STDs of the GPS and GLONASS combined corrections, including the satellite clocks, L1 satellite phase biases, and slant ionospheric delays at station BRCH, estimated by the code-plus-phase ionosphere-weighted model using the data from the network of homogeneous receivers on day 001 of 2019

those of satellite clocks and phase biases, indicating that the precision of ionospheric corrections is also far from the precision of phase observations, especially during the period of initialization.

We now explain why the individual products with centimeter-level precision are sufficient to correct the phase observations with millimeter-level precision. As clarified in Khodabandeh and Teunissen (2015), the individual corrections are highly correlated. Therefore, evaluation of the qualities of the corrections separately is not advisable; rather, one should concentrate on the precision of the combined corrections. Figure 5 shows the formal STDs of the GPS and GLONASS combined corrections, including satellite clocks, satellite phase biases, and ionospheric delays. We see that the precision of the combined corrections is typically at the millimeter level. The variation in the STD time series is dominated by the change in satellite elevation angles. Reviewing the interpretation of each correction, as listed in Table 1, note that the sum of the estimable satellite clocks, satellite phase biases, and slant ionospheric delays equals the phase observations (Khodabandeh 2021), demonstrating that the precision of the combined corrections is indeed phase-dominated. The conclusion therefore is that the network products are suitable for the correction of both code and phase observations on the user side, even when a new satellite rises. Moreover, this is why the covariances between corrections are essential, except for the variances when using the network corrections.

3.2.2 User positioning

By means of corrections estimated by the network side, the PPP-RTK users can achieve ambiguity resolution and high-accuracy positioning. This section presents the benefits of integer ambiguity resolution, the contribution of GLONASS, and the advantages of adding ionospheric corrections. We first show the positioning errors of some stations (arbitrarily chosen) and then offer the statistical results of all five-day datasets collected at 12 user stations. The example results at the arbitrarily chosen stations serve to show the details of the positioning error time series, while the statistical results help us consolidate the discoveries. The positioning error is defined as the difference between our epochal PPP-RTK positioning solution and the one-week static solution provided by the Natural Resources Canada's Canadian Spatial Reference System (CSRS) PPP services (Banville et al. 2021).

Figure 6 provides a comparison between the ambiguity-float and ambiguity-fixed solutions calculated by the code-plus-phase ionosphere-float model using GPS + GLONASS observations collected at station MILI on day 003 of 2019. When focusing on the left panel, which shows the results of the first hour, we see that the positioning errors of the ambiguity-float solution decrease gradually with the accumulation of observations, whereas the time series of the ambiguity-fixed solution present a sudden reduction. This sudden reduction indicates the time to first fix (TTFF) since the positioning errors at that time reach the centimeter level, which is much smaller than the positioning errors of the

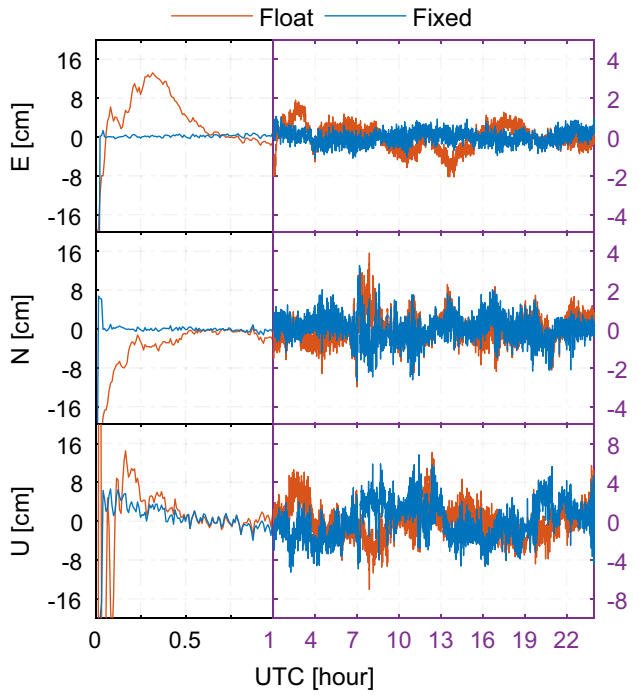

Fig. 6 Positioning errors of the ambiguity-float and ambiguity-fixed solutions calculated by the code-plus-phase ionosphere-float model using the GPS + GLONASS observations collected at station MILI (located in the network of homogeneous receivers) on day 003 of 2019

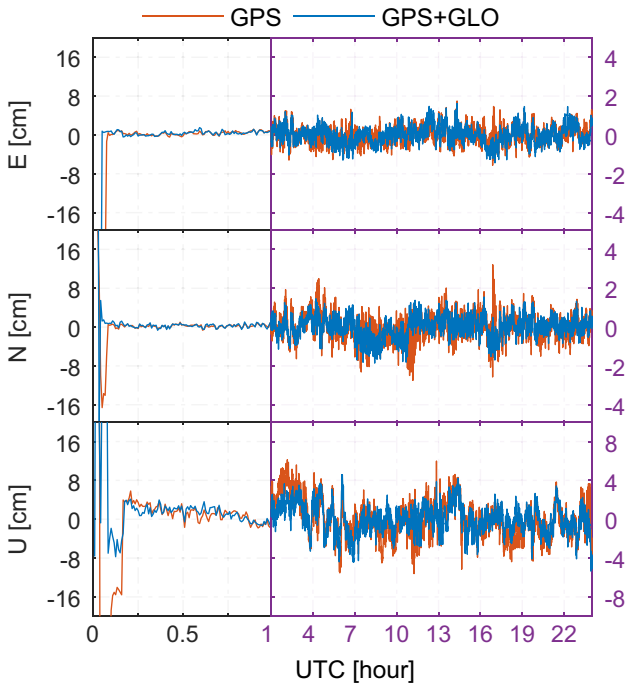

Fig. 7 Positioning errors of the ambiguity-fixed GPS and GPS + GLONASS (GPS + GLO) solutions calculated by the code-plus-phase ionosphere-float model using the observations collected at station MINH (located in the network of homogeneous receivers) on day 003 of 2019

ambiguity-float solution, especially on the horizontal components. We thus point out that the first benefit of ambiguity resolution lies in speeding up the convergence. The second benefit, as illustrated in the right panel, is improving the positioning accuracy, mainly on the east component. We see that the time series of the east component ambiguity-float positioning are noisier than those of the ambiguity-fixed solution. The improvement on the north and up components is less remarkable than that on the east component, which is consistent with the fact that the ambiguity resolution mainly improves the positioning accuracy on the east component (Ge et al. 2008). Here and in the following, we define the convergence time as the minimum observation time span required to achieve and maintain positioning errors better than 10 cm for at least 60 min. For the ambiguity-fixed solution, the convergence time also indicates the TTFF since the positioning errors reach centimeter level once the ambiguities are successfully fixed.

By comparing the GPS + GLONASS ambiguity-fixed solution with the ambiguity-float solution, we have demonstrated the benefits of integer ambiguity resolution. To investigate whether GLONASS contributes to ambiguity-fixed positioning, we now compare the ambiguity-fixed dual-system results with the GPS-only results, which are shown for station MINH in Fig. 7. From the left panel, we see that the convergence time of the dual-system positioning is ahead of that of GPS-only positioning. On the other hand, the right panel shows that the time series of the dual-system results vary almost within the time series of the GPS-only results, indicating that adding GLONASS observations improves the positioning accuracy. Here, we show only the results of one station on one day to indicate the improvement brought by adding GLONASS observations. We provide the statistical results of all five-day datasets collected at the 12 stations to consolidate the contribution of GLONASS at the end of this section.

To further improve the positioning, users can make use of the ionospheric products and switch the ionosphere-float variant to the ionosphere-weighted variant. Figure 8 shows the positioning errors of the ionosphere-float and ionosphere-weighted ambiguity-fixed solutions using the GPS + GLONASS code and phase observations at station METR on day 003 of 2019. It is impressive to see instantaneous centimeter-level positioning on the horizontal components when using the ionosphere-weighted variant, which is unachievable for users employing the ionosphere-float variant, as convergence takes several minutes. Concerning the vertical component, although the positioning based on the ionosphere-weighted variant converges to the centimeter level after several epochs, its initialization time is shorter

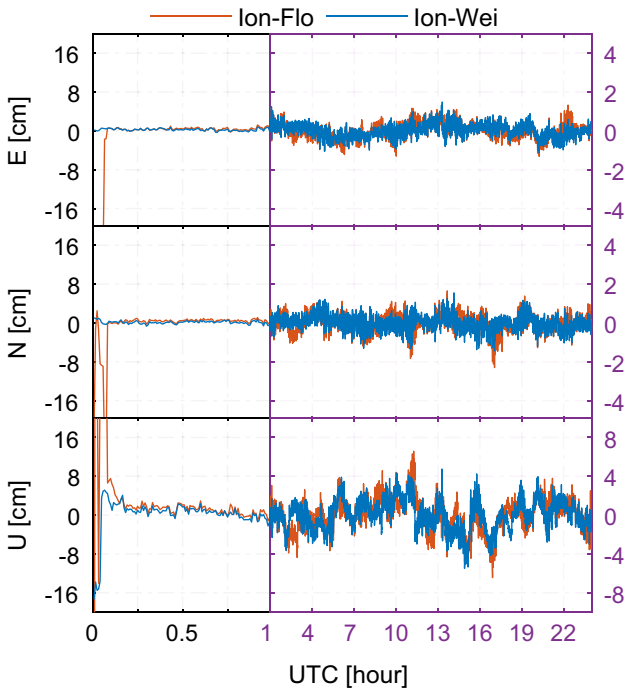

Fig. 8 Positioning errors of the ionosphere-float (Ion-Flo) and ionosphere-weighted (Ion-Wei) ambiguity-fixed solutions using the GPS + GLONASS code and phase observations at station METR (located in the network of homogeneous receivers) on day 003 of 2019

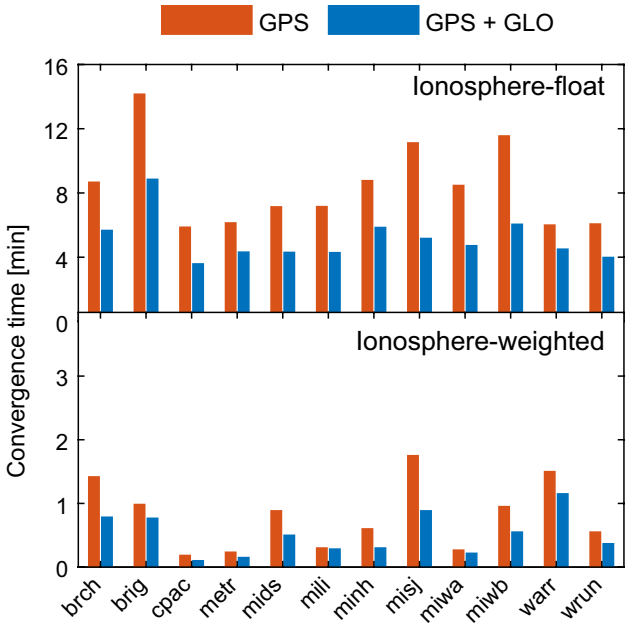

Fig. 9 Average convergence time of the five-day GPS and GPS + GLONASS ambiguity-fixed positioning errors at each station in the network of homogeneous receivers. The two panels show the results based on the code-plus-phase ionosphere-float (top) and ionosphere-weighted (bottom) models

than that based on the ionosphere-float variant. After initialization, the positioning time series of the two models are quite similar, implying no remarkable improvement in accuracy when adding ionospheric corrections. This result occurs because the positioning accuracy of ionospheric-float PPP-RTK with long-time-span observations is already high thanks to the ambiguity resolution. We thus conclude that ionosphere-weighted PPP-RTK converges faster than ionosphere-float PPP-RTK and that both have comparable positioning accuracies after convergence.

We now turn to the five-day statistical results at each station. Figure 9 shows the average convergence time. To make the results more reliable, we reprocessed the data by reinitiating the filter every 4 h. The convergence times presented here (and in Fig. 16) are the averages of 30 values over five days. The top panel of Fig. 9 indicates that, regarding ionosphere-float PPP-RTK, adding GLONASS observations shortens the convergence time from 6–14 to 4–8 min. In regard to the ionosphere-weighted PPP-RTK, as the bottom panel of Fig. 9 shows, the convergence times of the GPS-only and GPS + GLONASS results are under 2 and 1 min, respectively, also indicating the contribution of GLONASS. Comparing the results shown in the two panels of Fig. 9, ionosphere-weighted PPP-RTK converges faster than ionosphere-float PPP-RTK. For instance, the convergence time of GPS-only ionosphere-float PPP-RTK at station MIWA is 8 min, whereas only 0.5 min is required for ionosphere-weighted PPP-RTK.

Figure 10 depicts the root-mean-square (RMS) of the positioning errors per component at each station, where the error is the difference between our epochal PPP-RTK solution and the one-week static solution calculated by the CSRS-PPP (Banville et al. 2021). We here show the average RMS of the five-day data, in which the first hour of each day is taken out to exclude the results of initialization. When the GPS + GLONASS results are compared with the GPS-only results, an improvement in the RMS is noticeable on three components. The improvement on the vertical component is more significant than that on the horizontal component since the horizontal accuracy of GPS-only positioning is already high thanks to the ambiguity resolution. The accuracy of ionosphere-float and ionosphere-weighted PPP-RTK is overall comparable after convergence, as the RMS at all stations is almost at the same level, except that at station WARR, where the accuracy of ionosphere-float PPP-RTK is slightly higher than that of ionosphere-weighted PPP-RTK. This discrepancy occurs because this station is at the edge of the network and the error of ionospheric interpolation involved in the ionosphere-weighted model affects the positioning. However, the ionosphere-weighted PPP-RTK at this station still converges faster as shown in Fig. 9. Overall, the ionosphere-weighted PPP-RTK converges faster than

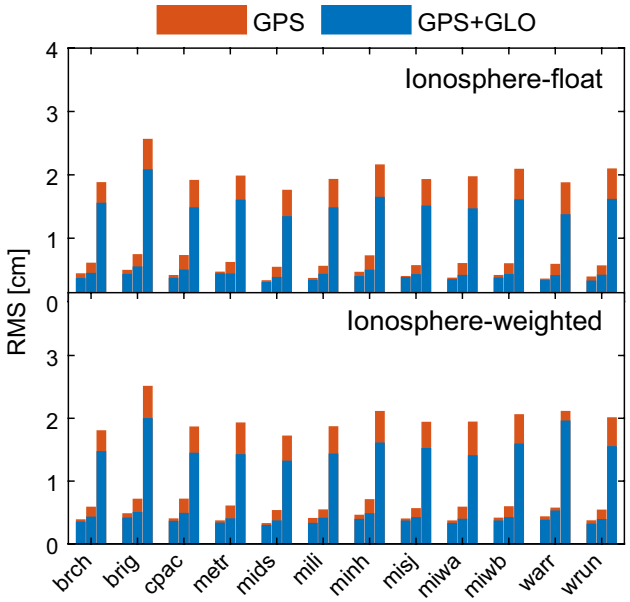

Fig. 10 Average RMS of the five-day GPS and GPS + GLONASS ambiguity-fixed positioning at each station in the network of homogeneous receivers. The two panels show the results based on the code-plus-phase ionosphere-float (top) and ionosphere-weighted (bottom) models. The three bars at each station represent the RMS on the east, north, and up components

the ionosphere-float PPP-RTK, and both have comparable positioning accuracies after convergence.

Finally, Table 8 summarizes the average convergence times and RMSs of all stations. We here conclude three findings. First, the ambiguity resolution speeds up the convergence and improves the accuracy, especially for the east component. For instance, in the ionosphere-float GPS + GLONASS results, the ambiguity-fixed solution converges in 5 min and reaches an accuracy of 3.6 mm on the east component compared to the convergence time of 11 min and RMS of 5.9 mm of the ambiguity-float solution. Second, integrating GLONASS with GPS improves the positioning performance compared to that of GPS-only case. We see a reduction of 20–50% in convergence time and an improvement of 8–45% in positioning accuracy when comparing the dual-system results with the GPS-only results. Third, the ionosphere-weighted variant outperforms the ionosphere-float variant, mainly owing to the shortening of the convergence time. The convergence time is shortened from 5–8.5 to 0.5–1 min when switching the ionosphere-float variant to the ionosphere-weighted variant.

3.3 Network equipped with heterogeneous receivers

By processing the data collected in the network equipped with heterogeneous receivers, in this section, we test the phase-only GLONASS model. We successively analyze the network products and user positioning.

3.3.1 Network products

The network side processing the GLONASS phase data provides only satellite clocks and ionospheric corrections, the analytical forms of which are different from those estimated by the code-plus-phase model. We provide insights into the characteristics and precision of GLONASS products estimated by the phase-only model and compare them with the GPS products estimated by the code-plus-phase model.

Figure 11 shows the GPS and GLONASS satellite clocks together with their formal STDs on day 356 of 2019. Despite the differences between the analytical forms of the GPS and GLONASS satellite clocks, both exhibit a similar linear trend. However, their formal STDs are quite different. The precision of the GLONASS satellite clocks generally reaches two-centimeter level, whereas the STDs of the GPS satellite clocks are much larger. However, this does not imply the outperformance of the phase-only model. The estimable satellite clocks based on the two models are different, and assessment of the quality of corrections separately is not advisable, as demonstrated earlier. We show the precision of the combined corrections estimated by the two models after depicting the time series of the ionospheric corrections.

Table 8 Average convergence (Con.) time and RMS of all stations equipped with homogeneous receivers

Model	System	Ambiguity-float solution				Ambiguity-fixed solution			
		Con. (min)	RMS (mm)			Con. (min)	RMS (mm)		
			E	N	U		E	N	U
Ionosphere-float	GPS	16	9.5	8.3	20.3	8.5	3.9	6.1	20.1
	GPS + GLONASS	11	5.9	4.6	16.1	5	3.6	4.4	15.6
	Improvement (%)	31	38	45	21	41	8	28	22
Ionosphere-weighted	GPS	10	8.2	7.4	19.8	1	3.9	6.0	19.8
	GPS + GLONASS	8	6.2	5.0	16.3	0.5	3.5	4.3	15.5
	Improvement (%)	20	24	32	18	50	10	33	22

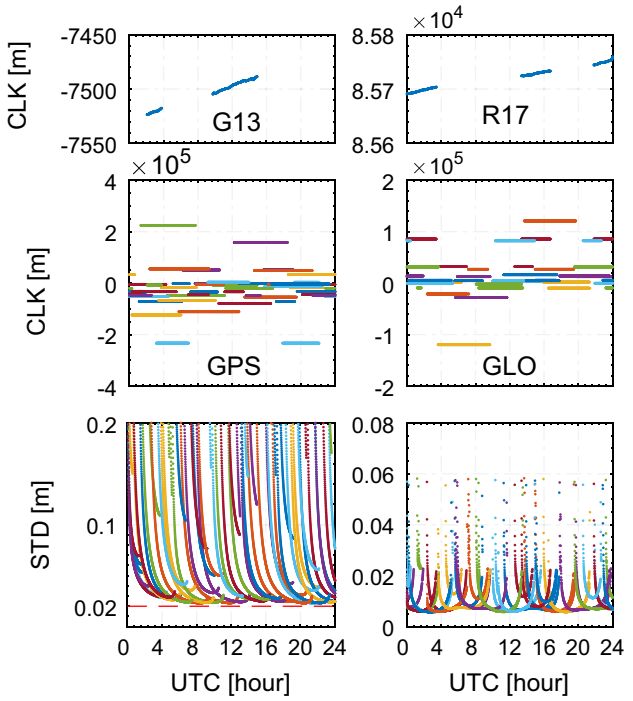

Fig. 11 GPS and GLONASS satellite clocks together with their formal STDs obtained by using the data from the network of heterogeneous receivers on day 356 of 2019. The GPS data are processed by the code-plus-phase ionosphere-float model, while the GLONASS data are processed by the phase-only ionosphere-float model

Figure 12 shows the GPS and GLONASS slant ionospheric delays at station CTEG together with their formal STDs on day 356 of 2019. We see that the characteristics of the GPS and GLONASS slant ionospheric delays are still similar. The difference between the GPS and GLONASS slant ionospheric delays lies in their formal STDs. The precision of the GLONASS slant ionospheric delay is dominated by phase observations and presents an elevation-dependent trend, while the precision of GPS slant ionospheric delays decreases gradually and reaches the centimeter level after 1 h.

Although the precision of individual satellite clocks and ionospheric delays is at the centimeter level, it is still larger than the precision of the phase observations. This is due to the strong correlation existing between the estimable satellite clocks and ionospheric delays based on the phase-only model. We thus calculate the precision of the combined corrections. As shown in Fig. 13, the GLONASS time series are typically under 0.01 m, as are the GPS time series, and therefore are precise enough for user correction. We note that the combined corrections estimated by the phase-only model actually include the satellite clocks, satellite phase biases, and ionospheric delays since the estimable satellite clocks are lumped with the original satellite clocks and the satellite phase biases.

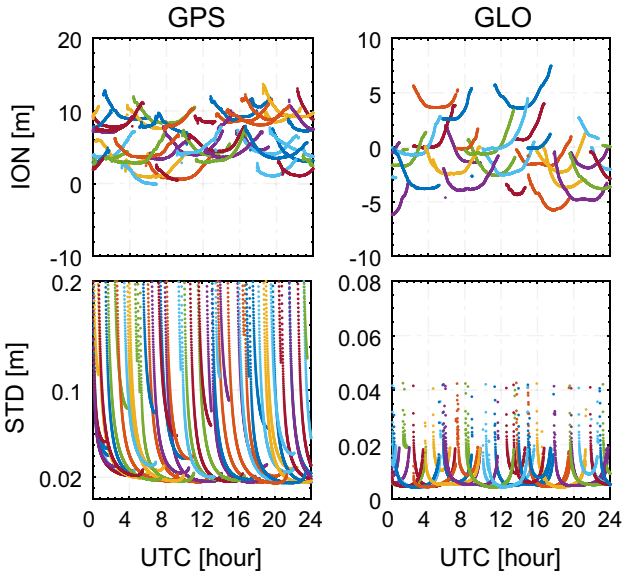

Fig. 12 GPS and GLONASS slant ionospheric delays at station CTEG together with their formal STDs obtained by using the data from the network of heterogeneous receivers on day 356 of 2019. The GPS data are processed by the code-plus-phase ionosphere-weighted model, while the GLONASS data are processed by the phase-only ionosphere-weighted model

3.3.2 User positioning

This subsection aims to analyze the positioning performance in a network equipped with heterogeneous receivers and

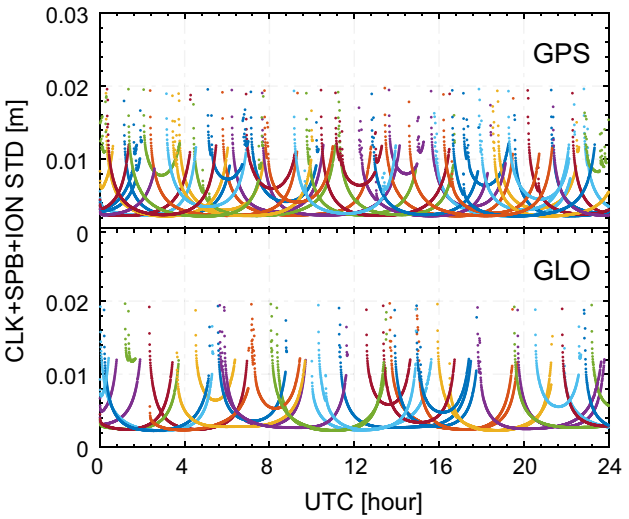

Fig. 13 Formal STDs of the GPS and GLONASS combined corrections, including the satellite clocks, satellite phase biases, and slant ionospheric delays at station CTEG obtained by using the data from the network of heterogeneous receivers on day 356 of 2019. The GPS data are processed by the code-plus-phase ionosphere-weighted model, while the GLONASS data are processed by the phase-only ionosphere-weighted model

investigate whether adding only GLONASS phase observations improves the positioning compared to the GPS-only solution. Along a similar line, we first give the results at some stations and then show the statistical results of all datasets.

Figure 14 shows the positioning errors of GPS and GPS + GLONASS positioning based on the ionosphere-float model using the observations collected at station NYKT on day 358 of 2019. The left three panels show that the ambiguity-float positioning errors gradually approach zero and that the convergence time of the GPS + GLONASS solution is shorter than that of the GPS-only solution. As shown in the right panels, a sudden reduction occurs, implying successful ambiguity in both the GPS-only and GPS + GLONASS ambiguity-fixed time series. The TTFF of GPS + GLONASS positioning is shorter than that of GPS-only positioning. We thus conclude that adding only GLONASS phase observations can also speed up the initialization, regardless of whether the ambiguities are fixed. On the other hand, we see that the time the ambiguity-fixed solution requires to reach centimeter-level positioning is less than that required by the ambiguity-float solution, which demonstrates the benefit of the ambiguity resolution.

As demonstrated before, GPS-only ambiguity-fixed positioning based on the ionosphere-weighted model already converges rapidly and becomes more promising if the addition of GLONASS phase observations can improve the positioning accuracy. Figure 15 shows the positioning errors of the ambiguity-fixed GPS and GPS + GLONASS solutions calculated by the ionosphere-weighted variant using the observations collected at station CTBR on day 358 of 2019. As we expected, the noise of the GPS + GLONASS time series is smaller than that of the GPS time series, especially on the north and up components, indicating the contribution of the GLONASS phase observations. The improvement on the east component is not remarkable, since the east positioning accuracy is already high due to the integer ambiguity resolution.

To further verify the contribution of GLONASS, we assess the positioning performance at all stations. Figures 16 and 17, respectively, show the average convergence time and RMS of five-day GPS and GPS + GLONASS ambiguity-fixed positioning at each station. Figure 16 indicates that the GPS + GLONASS solution converges faster than the GPS-only solution; in both two cases, the ionosphere-float and ionosphere-weighted models are adopted. Taking advantage of the ionospheric corrections, the ionosphere-weighted model outperforms the ionosphere-float model in terms of the convergence time. Figure 17 demonstrates the contribution of GLONASS in terms of the positioning accuracy, as indicated by the smaller RMS of the GPS + GLONASS solution than that of the GPS-only solution. Comparing the results in the two panels illustrates that the positioning

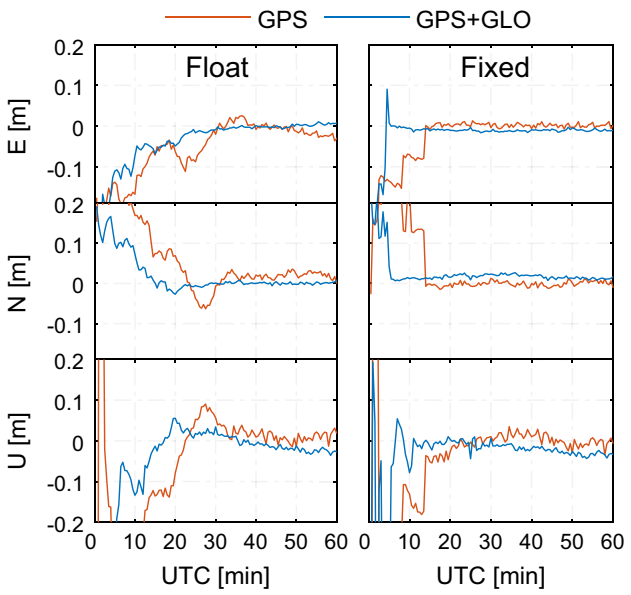

Fig. 14 Positioning errors of the GPS (code-plus-phase) and GPS (code-plus-phase) + GLONASS (phase-only) solutions calculated by the ionosphere-float model using the observations collected at station NYKT (located in the heterogeneous network) on day 358 of 2019

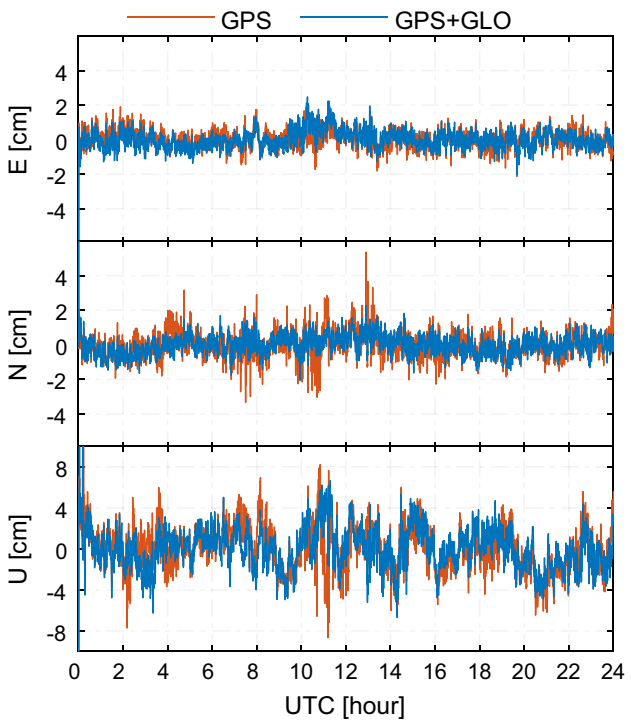

Fig. 15 Positioning errors of the ambiguity-fixed GPS (code-plus-phase) and GPS (code-plus-phase) + GLONASS (phase-only) solutions calculated by the ionosphere-weighted model using the observations collected at station CTBR (located in the heterogeneous network) on day 358 of 2019

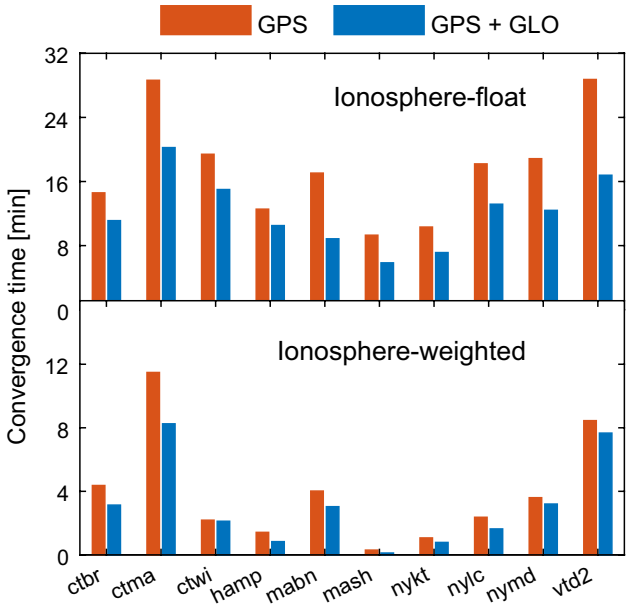

Fig. 16 Average convergence time of the five-day GPS (code-plus-phase) and GPS (code-plus-phase) + GLONASS (phase-only) ambiguity-fixed positioning at each station in the heterogeneous network. The two panels show the results based on the ionosphere-float (top) and ionosphere-weighted (bottom) models

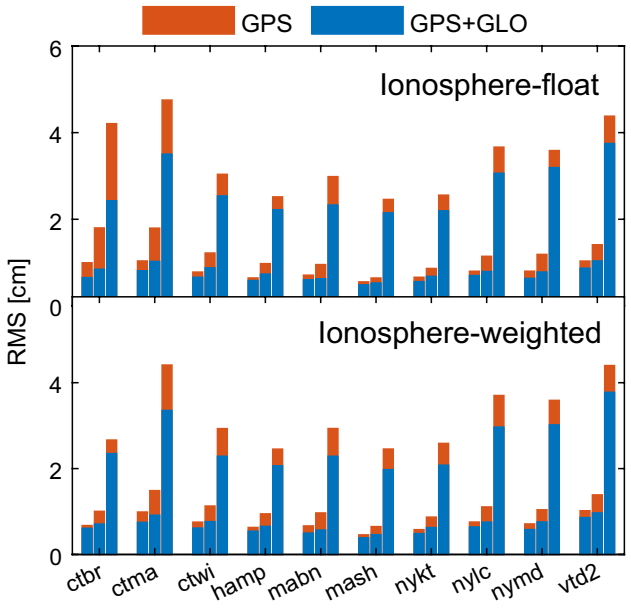

Fig. 17 Average RMS of the five-day GPS (code-plus-phase) and GPS (code-plus-phase) + GLONASS (phase-only) ambiguity-fixed positioning errors at each station in the heterogeneous network. The two panels show the results based on the ionosphere-float (top) and ionosphere-weighted (bottom) models. The three bars at each station present the RMS on the east, north, and up components

accuracies of ionosphere-float and ionosphere-weighted PPP-RTK are comparable.

Table 9 provides the average convergence time and RMS of all stations equipped with heterogeneous receivers. It again substantiates the benefits of the ambiguity resolution, the contribution of GLONASS, and the outperformance of the ionosphere-weighted variant. Among these three discoveries, we clarify that the contribution of GLONASS here resorts only to its phase observations, whereas the contribution of both GLONASS code and phase observations was demonstrated earlier in Table 8. Comparing the results listed in Tables 8 and 9, we see that the positioning performance in the network equipped with homogeneous receivers is better. Since the quality of observation is receiver-specific (Bona 2000; Zhang et al. 2020), the establishment of a more realistic stochastic model for all types of receivers in the heterogeneous network is worthwhile, thereby improving the positioning. This will be carried out in a future study. Finally, we clarify that the convergence performance reported in this study is based on the GPS/GLONASS data of a 30-s sampling interval. We have also carried out some experiments in a network that collected 1 Hz data. The results (although not shown here) indicated that PPP-RTK with 1 Hz data did speed up the convergence compared with PPP-RTK with 30-s data, mainly for the up component.

4 Conclusions

In this contribution, we presented a GLONASS PPP-RTK concept by taking advantage of the integer-estimable frequency division multiple access (IE-FDMA) model proposed in (Teunissen 2019) to ensure the rigor of the GLONASS integer ambiguity resolution. In the case of a network equipped with homogeneous receivers, we extended the well-known common clock PPP-RTK model to GLONASS FDMA signals, in which the inter-frequency biases (IFBs) can be implicitly eliminated since the common clock model parameterizes the biases in a between-receiver differenced form. In a network equipped with heterogeneous receivers, we used only the phase observables and developed a phase-only IE-FDMA GLONASS PPP-RTK model, thereby circumventing the inverse effects of IFBs. For verification purposes, we collected a set of five-day global positioning system (GPS) and GLONASS data in two networks: one equipped with homogeneous receivers and another equipped with heterogeneous receivers. The main findings based on the experimental results are as follows.

On the network side, the GLONASS-specific corrections, including satellite clocks, satellite phase biases, and ionospheric delays, were as precise as those of their GPS-specific counterparts. Both GPS and GLONASS network products were qualified to correct the observables on the

Table 9 Average convergence (Con.) time and RMS of all stations equipped with heterogeneous receivers

Model	System	Ambiguity-float solution				Ambiguity-fixed solution			
		Con. (min)	RMS (mm)			Con. (min)	RMS (mm)		
			E	N	U		E	N	U
Ionosphere-float	GPS	28	22.4	15.7	40.1	18	7.8	12.0	39.2
	GPS + GLONASS	18	8.8	8.2	28.3	12	6.6	7.9	27.4
	Improvement (%)	36	61	48	29	33	15	34	30
Ionosphere-weighted	GPS	13.5	16.8	15.1	35.7	4	7.2	10.6	35.6
	GPS + GLONASS	9	8.6	8.1	26.8	3	6.0	7.2	26.2
	Improvement (%)	33	49	46	25	25	17	32	26

user side, although the precision of the individual corrections was several centimeters. We substantiated that due to the strong correlation existing between individual corrections, the quality of network corrections must be evaluated by using the precision of combined corrections. After forming the combined corrections, the formal standard deviation reached the millimeter level and was thus precise enough for user positioning.

On the user side, we demonstrated the benefits of the integer ambiguity resolution, the contribution of GLONASS, and the advantages of adding ionospheric corrections. Based on the IE-FDMA model, we succeeded in fixing both GPS and GLONASS ambiguities with the aid of satellite phase biases, leading to improved positioning compared to the ambiguity-float results. The convergence time was shortened from 11 (18) to 5 (12) min in the network equipped with homogeneous (heterogeneous) receivers. For the ambiguity-fixed results, the convergence time defined in this work also indicates the time to first fix since the positioning error converges to the centimeter level once the ambiguities are successfully fixed. The improvement in positioning accuracy was also remarkable, mainly on the east component, where the RMS decreased from 5.9 (8.8) to 3.6 (6.6) millimeters. We thus concluded that the IE-FDMA PPP-RTK model enables rigorous GLONASS ambiguity resolution, thereby shortening the convergence time and improving the positioning accuracy.

To demonstrate the contribution of GLONASS, we compared the performance of GPS + GLONASS positioning with that of GPS-only positioning. When adding both code and phase GLONASS observables, as in the network equipped with homogeneous receivers, the convergence time was shortened by 41%, and the positioning accuracy was improved by 8–28%. Interestingly, the results in the network equipped with heterogeneous receivers showed an improvement of the same extent, although only GLONASS phase observables were added. This result verifies that the contribution of GLONASS is phase-dominated. In other words, the improvement originating from the code observables is marginal. The results also demonstrate that the weakness of the phase-only GLONASS model can be remedied by integrating GLONASS phase observables with code division multiple access (CDMA) observables.

Providing users, among others, with ionospheric corrections further speeds up the initialization of the positioning. The GPS + GLONASS ionosphere-aided PPP-RTK positioning, namely, the positioning based on the ionosphere-weighted model, converged after 0.5 and 3 min in two networks. More impressively, instantaneous centimeter-level positioning on horizontal components was attainable at some stations. With respect to the positioning accuracy, the gain from adding ionospheric corrections was not that remarkable after initialization, since the accuracy of GPS + GLONASS positioning was already high thanks to the integer ambiguity resolution.

This study offers experience in the use of the IE-FDMA model in the context of GLONASS PPP-RTK and facilitates our understanding of the GLONASS integer ambiguity resolution. The proposed GLONASS PPP-RTK concept is also applicable to a global network, although our experimental analysis was limited to regional networks. We believe that integrating GLONASS with, aside from GPS, more systems such as the Chinese BeiDou and the European Galileo can further improve PPP-RTK positioning.

Acknowledgements This work was partially funded by the National Natural Science Foundation of China (Grant Nos. 42022025, 41774042) and the Scientific Instrument Developing Project of the Chinese Academy of Sciences (Grant No. YJKYYQ20190063). The corresponding author is supported by the CAS Pioneer Hundred Talents Program.

Author contributions BZ proposed the method, designed the research, and wrote the manuscript. PH developed the software, processed the data, and wrote the manuscript. JZ helped process the data. TL revised the manuscript. All authors contributed to the analysis, interpretation, and discussion of the results.

Data availability The RINEX data acquired from the National Geodetic Survey (NGS) CORS network in the USA can be downloaded at ftp://geodesy.noaa.gov/cors/.

References

Al-Shaery A, Zhang S, Rizos C (2013) An enhanced calibration method of GLONASS inter-channel bias for GNSS RTK. GPS Solutions 17(2):165–173

Baarda W (1973) S-transformations and criterion matrices. In: Publications on geodesy, 18 (vol 5, no 1), Netherlands Geodetic Commission, Delft, The Netherlands

Banville S, Collins P, Lahaye F (2013a) Concepts for undifferenced GLONASS ambiguity resolution. In: Proceedings of the 26th international technical meeting of the satellite division of the institute of navigation (ION GNSS+ 2013). Nashville, Tennessee, 16–20 September, pp 1186–1197

Banville S, Collins P, Lahaye F (2013b) GLONASS ambiguity resolution of mixed receiver types without external calibration. GPS Solut 17(3):275–282

Banville S et al (2021) Enabling ambiguity resolution in CSRS-PPP. NAVIG J Inst Navig 68(2):433–451

Blewitt G (1990) An automatic editing algorithm for GPS data. Geophys Res Lett 17(3):199–202

Bona P (2000) Precision, cross correlation, and time correlation of GPS phase and code observations. GPS Solut 4(2):3–13

Brack A, Männel B, Schuh H (2020) GLONASS FDMA data for RTK positioning: a five-system analysis. GPS Solut 25(1):1–13. https://doi.org/10.1007/s10291-020-01043-5

Collins P, Bisnath S, Lahaye F, Héroux P (2010) Undifferenced GPS ambiguity resolution using the decoupled clock model and ambiguity datum fixing. NAVIG J Inst Navig 57(2):123–135

Ge M, Gendt G, Ma R, Shi C, Liu J (2008) Resolution of GPS carrier-phase ambiguities in precise point positioning (PPP) with daily observations. J Geod 82(7):389–399

Geng J, Bock Y (2016) GLONASS fractional-cycle bias estimation across inhomogeneous receivers for PPP ambiguity resolution. J Geod 90(4):379–396

Hou P, Zhang B, Liu T (2020) Integer-estimable GLONASS FDMA model as applied to Kalman-filter-based short-to long-baseline RTK positioning. GPS Solut 24(4):1–14. https://doi.org/10.1007/s10291-020-01008-8

Hu J, Zhang X, Li P, Ma F, Pan L (2020) Multi-GNSS fractional cycle bias products generation for GNSS ambiguity-fixed PPP at Wuhan University. GPS Solut 24(1):1–13. https://doi.org/10.1007/s10291-019-0929-9

Khodabandeh A (2021) Single-station PPP-RTK: correction latency and ambiguity resolution performance. J Geod 95(4):1–24. https://doi.org/10.1007/s00190-021-01490-z

Khodabandeh A, Teunissen P (2015) An analytical study of PPP-RTK corrections: precision, correlation and user-impact. J Geod 89(11):1109–1132

Khodabandeh A, Teunissen P (2016) PPP-RTK and inter-system biases: the ISB look-up table as a means to support multi-system PPP-RTK. J Geod 90(9):837–851

Kozlov D, Tkachenko M, Tochilin A (2000) Statistical characterization of hardware biases in GPS+ GLONASS receivers. In: Proceedings of the 13th international technical meeting of the Satellite Division of The Institute of Navigation (ION GPS 2000). Salt Lake City, UT, 19–22 September, pp 817–826

Laurichesse D, Mercier F, Berthias JP, Broca P, Cerri L (2009) Integer ambiguity resolution on undifferenced GPS phase measurements and its application to PPP and satellite precise orbit determination. Navigation 56(2):135–149

Leandro R, Santos M, Langley R UNB neutral atmosphere models: development and performance. In: Proceedings of the 2006 national technical meeting of the institute of navigation. pp 564–573

Leick A, Rapoport L, Tatarnikov D (2015) GPS satellite surveying. Wiley, Hoboken

Li X, Li X, Yuan Y, Zhang K, Zhang X, Wickert J (2018) Multi-GNSS phase delay estimation and PPP ambiguity resolution: GPS, BDS, GLONASS. Galileo J Geod 92(6):579–608

Liu Y, Song W, Lou Y, Ye S, Zhang R (2017) GLONASS phase bias estimation and its PPP ambiguity resolution using homogeneous receivers. GPS Solut 21(2):427–437

Odijk D (2002) Fast precise GPS positioning in the presence of ionospheric delays. In: Publications on geodesy, 52, Netherlands Geodetic Commission, Delft, The Netherlands

Odijk D, Teunissen PJG, Zhang B (2012) Single-frequency integer ambiguity resolution enabled GPS precise point positioning. J Surv Eng 138(4):193–202

Odijk D, Zhang B, Khodabandeh A, Odolinski R, Teunissen PJG (2016) On the estimability of parameters in undifferenced, uncombined GNSS network and PPP-RTK user models by means of S-system theory. J Geod 90(1):15–44

Reussner N, Wanninger L (2011) GLONASS inter-frequency biases and their effects on RTK and PPP carrier-phase ambiguity resolution. In: Proceedings of ION GNSS 24th international technical meeting of the Satellite Division (ION GNSS 2011). Portland, OR, 19–23 September pp 712–716

Rocken C et al (1993) Sensing atmospheric water vapor with the Global Positioning System. Geophys Res Lett 20(23):2631–2634

Schönemann E, Becker M, Springer T (2011) A new approach for GNSS analysis in a multi-GNSS and multi-signal environment. J Geod Sci 1(3):204–214

Sleewagen J (2012) Demystifying GLONASS inter-frequency carrier phase biases. Inside GNSS 7(3):57–61

Takasu T, Yasuda A (2009) Development of the low-cost RTK-GPS receiver with an open source program package RTKLIB. In: International symposium on GPS/GNSS. Jeju, Korea, 4–6 November

Teunissen PJG (1985) Generalized inverses, adjustment the datum problem and S-transformations. In: Grafarend EW, Sanso F (eds) Optimization and design of geodetic networks. Springer, Berlin,

Teunissen PJG (1995) The least-squares ambiguity decorrelation adjustment: a method for fast GPS integer ambiguity estimation. J Geod 70(1–2):65–82

Teunissen P (1998) The ionosphere-weighted GPS baseline precision in canonical form. J Geodesy 72(2):107–111

Teunissen PJG (2019) A new GLONASS FDMA model. GPS Solut 23(4):1–19. https://doi.org/10.1007/s10291-019-0889-0

Teunissen PJG, Khodabandeh A (2015) Review and principles of PPP-RTK methods. J Geod 89(3):217–240

Teunissen PJG, Khodabandeh A (2019) GLONASS ambiguity resolution. GPS Solut 23(4):1–11. https://doi.org/10.1007/s10291-019-0890-7

Teunissen PJG, Montenbruck O (2017) Springer handbook of global navigation satellite systems. Springer, Berlin

Teunissen PJG, Odijk D, Zhang B (2010) PPP-RTK: results of CORS network-based PPP with integer ambiguity resolution. J Aeronaut Astronaut Aviat Ser A 42(4):223–230

Tian Y, Ge M, Neitzel F (2015) Particle filter-based estimation of inter-frequency phase bias for real-time GLONASS integer ambiguity resolution. J Geod 89(11):1145–1158

Wang K, Khodabandeh A, Teunissen P (2017) A study on predicting network corrections in PPP-RTK processing. Adv Space Res 60(7):1463–1477

Wanninger L (2012) Carrier-phase inter-frequency biases of GLONASS receivers. J Geod 86(2):139–148

Wübbena G, Schmitz M, Bagge A (2005) PPP-RTK: precise point positioning using state-space representation in RTK networks. In: Proceedings of the 18th international technical meeting of the satellite division of the institute of navigation (ION GNSS 2005). Long Beach, CA, 13–16 September, pp 13–16

Yamada H, Takasu T, Kubo N, Yasuda A (2010) Evaluation and calibration of receiver inter-channel biases for RTK-GPS/GLONASS. In: Proceedings of the 23rd international technical meeting of the satellite division of the institute of navigation (ION GNSS 2010). Portland, OR, 21–24 September, pp 1580–1587

Zhang B, Teunissen PJG, Odijk D (2011) A novel un-differenced PPP-RTK concept. J Navig 64(S1):S180–S191

Zhang B, Hou P, Liu T, Yuan Y (2020) A single-receiver geometry-free approach to stochastic modeling of multi-frequency GNSS observables. J Geod 94(4):1–21. https://doi.org/10.1007/s00190-020-01366-8